

www.advmattechnol.de

# Nanoarchitectonics of Two-Dimensional Electrochromic Materials: Achievements and Future Challenges

Meng Li, Zhenzhen Wu, Yuhui Tian, Feng Pan,\* Tim Gould,\* and Shanqing Zhang\*

Electrochromic effect has been discovered in many materials with a wide range of applications from visible to infrared, such as smart windows, electronic displays, infrared camouflage, and color-changeable tactile sensor. However, conventional electrochromic materials cannot meet the growing demand for electrochromic performance in terms of optical contrast, response time, durability, color diversity, and flexibility, which slows down developments in this area. This is mainly due to the limited number and variety of electrochromic materials. In strong contrast, nanoarchitectonics of 2D materials with atomically thin thickness, large lateral size, and diversified series can be an effective way to address these issues and improve the electrochromic performances. This review highlights the recent achievements of emerging 2D electrochromic materials, namely covalent organic frameworks, coordination nanosheets, and transition metal carbides/nitrides/carbonitrides (MXenes). The structures, electrochromic performances and their structure-performance relationship, and future challenges of these materials have been systematically explored. This review can pave a new avenue for the promotion of the nanoarchitectonic 2D materials for the up-scaled practical electrochromic applications.

M. Li, Z. Wu, Y. Tian, S. Zhang Centre for Catalysis and Clean Energy and School of Environment and Science Gold Coast Campus Griffith University Gold Coast, QLD 4222, Australia E-mail: s.zhang@griffith.edu.au M. Li, T. Gould Queensland Micro- and Nanotechnology Centre Nathan Campus Griffith University Brisbane, QLD 4111, Australia E-mail: t.gould@griffith.edu.au M. Li, F. Pan School of Advanced Materials Shenzhen Graduate School **Peking University** Shenzhen 518055, China E-mail: panfeng@pkusz.edu.cn



© 2022 The Authors. Advanced Materials Technologies published by Wiley-VCH GmbH. This is an open access article under the terms of the Creative Commons Attribution-NonCommercial-NoDerivs License, which permits use and distribution in any medium, provided the original work is properly cited, the use is non-commercial and no modifications or adaptations are made.

DOI: 10.1002/admt.202200917

# 1. Introduction

Electrochromism refers to the reversible and persistent changes of color, transmittance, or other optical properties through electrochemical redox reactions under applied voltage or current. As early as 1930,[1] tungsten oxide powders were found to be electrochemically reduced to blue in acidic solution. And reversible color changes were achieved by using sodium tungsten bronzes in 1951.[2] The first discovery of electrically induced electrochromic effects in tungsten oxide films was made in 1953.[3] Later, Deb obtained analogous results and published two widely known and cited papers in 1969 and 1973, [4,5] which are regarded as the beginning of research and development of electrochromic devices (ECDs). Currently, in the most widely adopted structure of ECDs (see Figure 1a), [6] electrochromic materials are sandwiched between transparent electrical conductors (electrodes) together with

conductive electrolytes. Under applied voltages, electrochromic materials undergo redox reactions and thereby the ECDs exhibit color changes as shown in Figure 1b. To date, electrochromic materials and ECDs have been used in a wide range of applications, such as smart windows, [7] electronic display, [8] radiative cooling materials, [9] camouflage, [10] and electronic skin. [11]

As the key component in ECDs, electrochromic materials can be traditionally divided into inorganic materials (transitional metal oxides), and organic materials. The latter include small organic molecules (viologen family), conducting polymers (polypyrrole, polythiophene, polyaniline, and their derivatives), and metal complexes (metal phthalocyanine, Prussian blue, and their derivatives). Their advantages and challenges in terms of electrochromic performance have been summarized in Figure 1c. For inorganic materials, tungsten oxide (WO<sub>3</sub>), the earliest discovered electrochromic material, plays a crucial role compared to others, such as NiO2, IrO2, Nb2O5, MoO3, Ta2O5,  ${\rm TiO_2}$ , and  ${\rm V_2O_5}$ .[3] The remarkable structure and cycling stability of inorganic materials attract considerable attention from academia to industry. However, the widespread adoption is hindered by disadvantages like slow switching speed, limited color types and modulation ranges, and high preparation cost of thin films. Organic electrochromic materials and metal complexes generally exhibit outstanding tunability of colors and optical properties, and structural diversity, while their long-term stability remains a major obstacle for large-scale applications, www.advancedsciencenews.com

www.advmattechnol.de

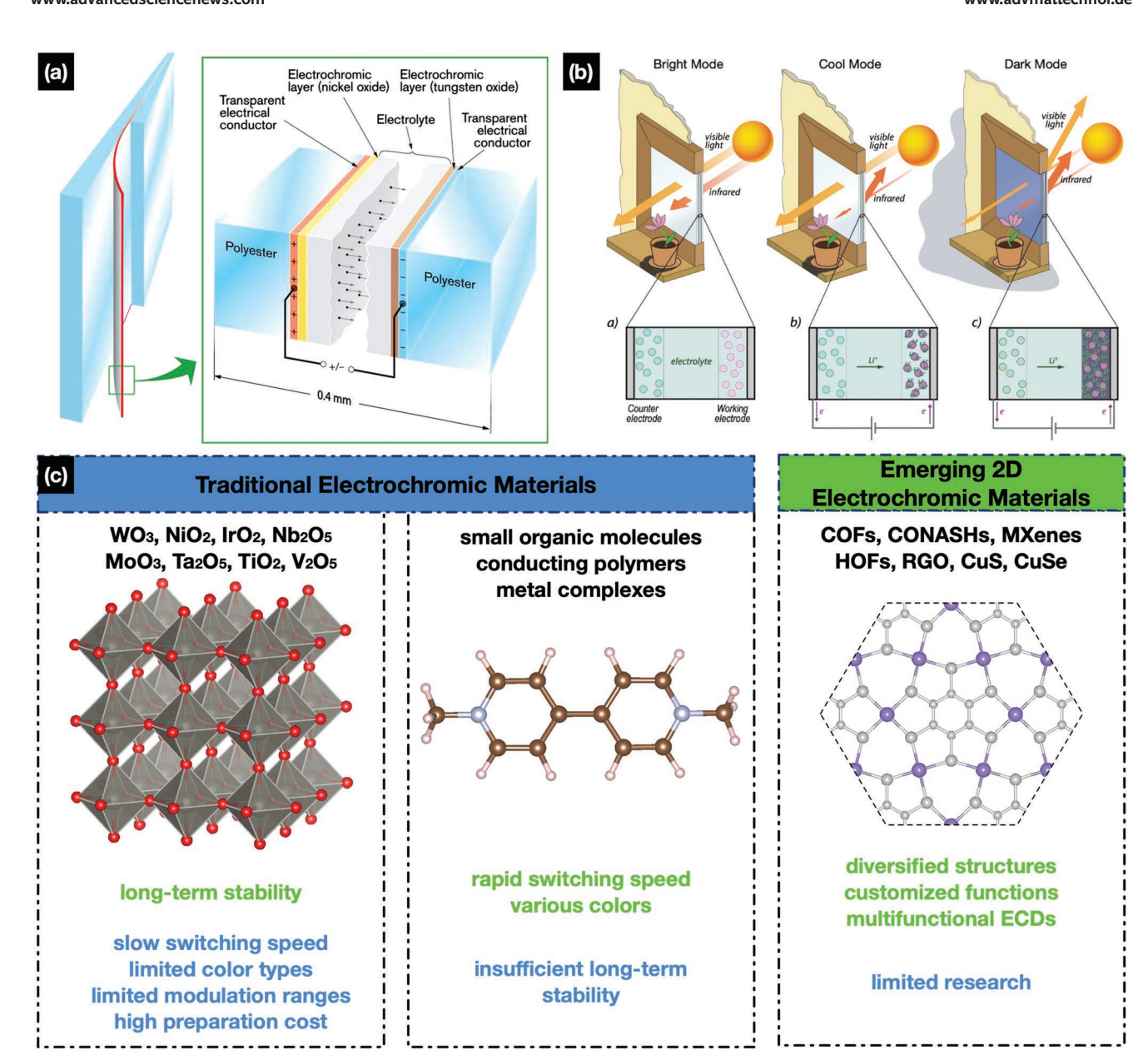


Figure 1. The structure and applications of typical electrochromic devices (ECDs): a) typical structure of a laminated ECD; (6) b) dual-band electrochromic windows. [7] c) The advantages (green) and challenges (blue) of traditional and emerging 2D electrochromic materials.

especially degradation under solar radiation with ultraviolet (UV) light. Numerous investigations have been implemented for practical applications in pursuit of better electrochromic performance, namely large optical contrast ( $\Delta T$ ), fast response time, high coloration efficiency (CE), low operating voltages, and long-term cycling stability.

Since 2014, as the most newly discovered materials, the electrochromic effects of reduced graphene oxide (RGO),[12] coordination nanosheets (CONASHs),[13] copper chalcogenides, [14,15] covalent organic frameworks (COFs), [16] transition metal carbides/nitrides/carbonitrides (MXenes),[17] and hydrogen-bonded organic frameworks (HOFs)[18] are reported in succession, which has significantly renewed research interest. The emerging 2D materials[19-24] exhibit unique

Adv. Mater. Technol. 2023. 8, 2200917

physical and chemical properties compared with traditional ones, and these differences may drastically improve the electrochromic performance in many cases. For example, the ultrahigh specific surface area and large van der Waals gap could accelerate ion transportation rates on the micro-level and switching speeds in ECDs on the macro. Notably, the diversified structures of these 2D materials greatly expand the range of electrochromic materials. And their periodic structures could facilitate understanding of the electrochromic mechanism at the molecular level via in situ spectra, X-ray diffraction (XRD), and even theoretical tools. The obtained structure-property relationship could be used to rationally design the nanoarchitectonics of 2D electrochromic materials with customized structures and functionalities. Consequently,

onlinelibrary.wiley.com/doi/10.1002/admt.202200917 by University Town Of Shenzhen, Wiley Online Library on [23/11/2025]. See the Terms

www.advancedsciencenews.com

www.advmattechnol.de

2D materials could become a promising ideal platform to satisfy diverse demands in electrochromism. To provide a better understanding, in this review, we summarize and refine recent advances in emerging 2D electrochromic materials, focusing on their structure-property relationship. Furthermore, we have discussed the merits and demerits of different groups of 2D electrochromic materials and research challenges for future electrochromic applications.

# 2. The Synthesis and Mechanism of Emerging **2D Electrochromic Materials**

#### 2.1. The Synthesis of Emerging 2D Electrochromic Materials

Emerging 2D electrochromic materials discovered so far include COFs, CONASHs, MXenes, HOFs, RGO, and copper chalcogenides, which are generally synthesized via two approaches, top-down and bottom-up (Figure 2). The former is to break interlayer interactions or chemical bonds via mechanical forces, sonication, and chemical or electrochemical reactions. Thus, this method only applies to 2D materials with existing bulk counterparts, such as MXenes and RGO. A common disadvantage of the top-down approach is the lack of flexibility in material properties, as it is difficult to tune properties through structural modification using this approach. In contrast,

the bottom-up approach is to build 2D materials from basic building blocks like metal atoms and ions, ligands, and molecules via various synthetic techniques, such as liquid-liquid interfacial synthesis, chemical vapor deposition (CVD), sol-gel methods, electrodeposition, electrospinning, and hydrothermal method. The bottom-up approach offers great capabilities in adjusting structures and properties of synthesized materials through design and choice of components, so many researchers prefer to adopt this method for material preparation.

#### 2.2. The Electrochromic Performance

Many synthesized thin films of 2D materials need to be transferred to substrates before testing in solutions (three-electrode systems) and/or ECDs (two-electrode systems) for evaluating electrochemical and electrochromic performance. In a typical three-electrode system, an electrochromic material deposited on a conductive substrate, usually a piece of indium tin oxide (ITO) glass, is used as the working electrode, with the counter and reference electrodes of blank ITO glass and Ag/AgCl, respectively. While for the ECD, two transparent electrodes are sandwiched through an electrolyte, with the electrochromic material deposited on one electrode. Among various parameters for describing the performance of ECDs, several key parameters are listed as follows. As ECDs in reflective mode are

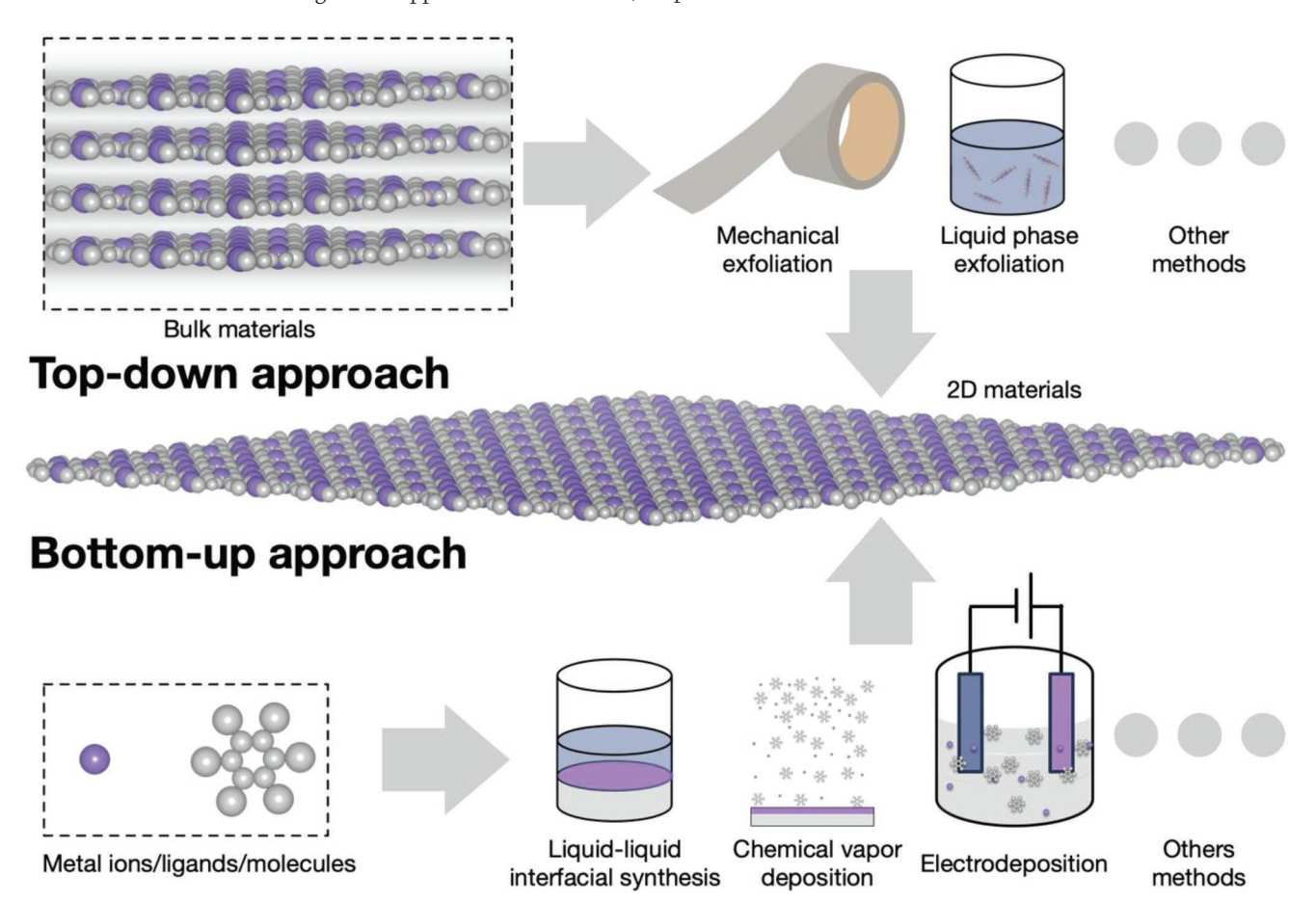


Figure 2. Schematic diagram for the synthesis of emerging 2D electrochromic materials via top-down and bottom-up approaches.

SCIENCE NEWS TECHNOLOGIES
www.advancedsciencenews.com
www.advancedsciencenews.com

not studied in the reviewed papers, all performance parameters are for transmittance mode in this review.

The optical contrast is one of the main parameters for ECDs, which is defined as the change of absorbance ( $\Delta A$ ) or transmittance ( $\Delta T$ ) in percentages between the colored ( $A_{\rm c}$ ,  $T_{\rm c}$ ) and bleached ( $A_{\rm b}$ ,  $T_{\rm b}$ ) states at a specific wavelength ( $\lambda_{\rm max}$ ), as shown in Equation (1):

$$\Delta T = T_b - T_c \text{ or } \Delta A = A_c - A_b \tag{1}$$

The optical contrast is dependent on the thickness of the prepared film and can reflect color changes during electrochromism to a large extent. ECDs with high optical contrasts are generally preferred for practical applications.

The response (switching) time (t) is an essential parameter for evaluating the color changing speed of an ECD, defined as the time needed for an ECD to switch between the bleached and colored states (or vice versa), corresponding to the optical contrast changing from 0% to 90% or 95% during electrochromic processes. The response time can be divided into coloration time  $(t_c)$  and bleaching time  $(t_b)$  with different values in most cases. This parameter is dependent on the ionic conductivity of electrolytes, ion diffusion distances, electronic conductivity of electrodes, morphology of active materials, and even voltage scanning rates. Thus, comparing the response abilities of different ECDs via response time is challenging and even meaningless for ECDs with large changes in optical properties. For practical applications like electrochromic displays, a short switching time is one of the basic requirements, while for smart windows, tens of seconds are usually acceptable as optical contrast and long-term stability are the top priorities under the circumstances.

CE is a practical parameter to evaluate the energy consumption for the electrochromic process that higher values mean larger color changes induced by the same amount of energy. CE  $(\eta)$  is defined as the ratio between changes of optical density  $(\Delta OD)$  or absorbance  $(\Delta A)$  at a specific wavelength  $(\lambda_{max})$  and inject charge unit area  $(Q_d)$ , as shown in Equation (2):

$$\eta = \frac{\Delta OD}{Q_d} = \frac{\Delta A}{Q_d} = \frac{\log(T_b/T_c)}{Q_d} \tag{2}$$

The unit of  $\eta$  and  $Q_{\rm d}$  is cm<sup>2</sup> C<sup>-1</sup> and C cm<sup>-2</sup>, respectively. Like response time, the CE value is calculated based on the 90% or 95% of the total optical contrast ( $\Delta T$ ). The types of electrochromic materials, charge insertion amount, and voltage programs affect the value of CE, and higher values are always well-received.

Long-term (cycling) stability determines the service life of ECDs, usually represented by maximum cycling number with neglectable decay in optical contrast ( $\Delta T$ ), which have no clear definition and depend on the types of applications. The long-term stability is mainly controlled by the reversibility of the corresponding electrochemical reactions, with related factors of electrodes, electrolytes, reaction rates, device structures, working temperatures, and applied voltages. An ideal cycling number is about  $10^4$ – $10^6$ , which is beyond the practical value of most discovered electrochromic materials, except inorganic oxides. This parameter becomes the main barrier to other groups of electrochromic materials for further development and one of the most critical factors that whether an electrochromic

material can be commercialized in large-scale. To prolong service life, ECDs are usually sealed to avoid the adverse effects of external air and water. It is still a challenge to improve the long-term stability of electrochromic materials, especially those suitable for various circumstances.

The memory effect is one of the most unique and attractive properties of electrochromic materials. Compared with other color-changeable electronic devices, ECDs consume a small amount of energy only in the switching processes, maintaining their color and optical properties for a period of time after removing the applied voltages at both colored and bleached states. The ideal duration is the longer, the better. The phenomenon of color recovery in practical ECDs is called self-erasing due to slow diffusion induced self-discharge. Thus, solid and semisolid state ECDs have been proposed to overcome this problem.

## 2.3. The Structure-Performance Relationship

The emerging 2D electrochromic materials have many unique structural characteristics, resulting in improvements in electrochemical and electrochromic performance. The structureperformance relationship of 2D electrochromic materials is illustrated in Figure 3. One of the unique characteristics of 2D materials is their intrinsic flexibility due to their atomically thin thickness. Meanwhile, the high specific surface area and 1D pore channels of some 2D materials could facilitate ion transportation by reducing diffusion distances and offering multiple diffusion pathways. The improved electrochemical performance is usually accompanied with improved reaction reversibility and capacity, resulting in large optical contrasts, high coloration efficiency, and rapid switching speeds. Moreover, the crystal morphology of 2D materials is based on longrange interlayer  $\pi$ - $\pi$  stacking, which could help keep efficient contact with electrodes, maintain structural integrity under

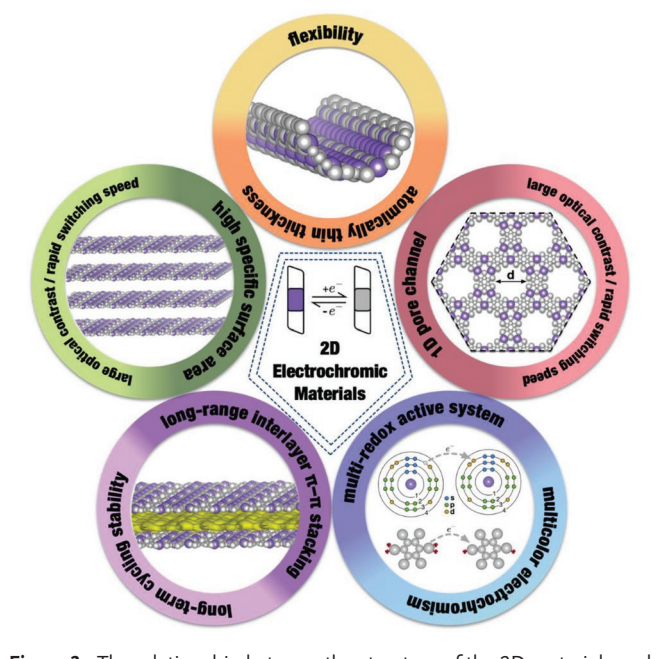


**Figure 3.** The relationship between the structure of the 2D materials and the electrochromic performances.

ADVANCED MATERIALS

www.advancedsciencenews.com www.advmattechnol.de

intercalation/deintercalation-induced deformations, and ensure long-term cycling stability. By selecting building blocks of redox-active metal ions and ligands, multi-redox active systems could be established with multicolor electrochromism.

# 3. The Emerging 2D Electrochromic Materials

#### 3.1. COFs

Organic materials of small molecules and conducting polymers are traditional electrochromic materials that have been studied for decades. They generally have excellent optical modulation ranges and diversified colors. However, their long-term durability becomes a significant obstacle for large-scale commercialization, especially thermal, light, and cycling stability. 2D COFs, consisting of organic redox-active building blocks and electronrich linkers, are gradually regarded as promising electrochromic materials with structures summarized in Figure 4. Due to the strong covalent bonds, COFs have a rigid structure with high crystallinity, resulting in excellent stability in the electrochemical processes. The periodic distribution of pores and layered structures form 1D diffusion channels for ions, which offers rapid ion transportation rates and electrochromic switching speed. And the quasi-aromatic feature of large-scale intralayer delocalized electrons provides high electron conductivity. According to the linker design strategy, a donor-acceptor-donor electronic setup can significantly enhance the intramolecular charge transfer (ICT) and light absorption coefficients from the visible to near-infrared (NIR) regions. These characteristics of 2D COFs provide a solid foundation for excellent cycling stability, electrochemical and electrochromic performance.

The first electrochromic effect discovered in 2D COFs was reported by Wang et al. in 2019.<sup>[16]</sup> They synthesized an oriented COF film (COF<sub>3PA-TT</sub>) directly on ITO glasses through the liquid/solid interface solvothermal method. The building blocks of tris(4-aminophenyl)amine (TAPA) and thieno[3,2-b] thiophene-2,5-dicarbaldehyde (TTDA) were orderly connected via imine condensation reaction (**Figure 5a**). CV analysis was performed in 0.1 mol L<sup>-1</sup> LiClO<sub>4</sub>/propylene carbonate (PC) solution, with two pairs of redox peaks of the COF<sub>3PA-TT</sub> film at 0.95–0.68 V and 1.30–0.82 V (Figure 5b). The electrochromic performance was tested by immersing the COF<sub>3PA-TT</sub> deposited ITO in a quartz cell with the electrolyte of 0.1 mol L<sup>-1</sup> LiClO<sub>4</sub>/PC solution. Corresponding absorbance spectra at 0 and 1.4 V are shown in Figure 5c, with photographs showing the reversible color change from deep red to dark brown. There were

two intense absorption peaks at 350 and 482 nm in the neutral state of the COF<sub>3PA-TT</sub> film, which were replaced by new peaks at 400 and 585 nm with an increase of the NIR region under the potential of 1.4 V. The absorption peaks between 400 and 600 nm originated from the charge transfer from the triarylamine to the thienothiophene-diimine units. While in the NIR region, the triphenylamine (TPA) units were oxidized to cation radicals, and the intervalence charge transfer (IVCT) effect among the radicals led to the changes in the absorption spectra. The COF<sub>3PA-TT</sub> film could achieve contrast ratios ( $\Delta T$ %) of 16% at 610 nm and 15% at 1300 nm, respectively, under double-potential-step chronoamperometry (-0.8 and +1.4 V vs Ag/AgCl). The 90% response time (coloring/bleaching) at 610 and 1300 nm were 18.5/7 and 20/2.5 s, respectively, with corresponding CE values of 104 and 56 cm<sup>2</sup> C<sup>-1</sup>, respectively. The electrochromic performance of amorphous 3PA-TT films was also investigated, and the electrochemical processes were almost irreversible with poor stability, while the COF<sub>3PA-TT</sub> film could still maintain obvious redox peaks after 500 cycles. A quasi-solid-state ECD was fabricated to evaluate the practical performance of COF<sub>3PA-TT</sub> film according to the structure in Figure 5d. The COF<sub>3PA-TT</sub>-deposited ITO performed as the working electrode and blank ITO glass as the counter electrode, with the electrolyte of a LiClO<sub>4</sub>-based polymer gel. Under cyclic potential in the range of -2.0 to 2.4 V, the ECD exhibited a switching color between deep red to dark brown (Figure 5e), with similar changes in absorbance spectra (Figure 5f) compared to the COF<sub>3PA-TT</sub> film in the solution. Corresponding optical contrast ( $\Delta T\%$ ) was increased to 21% at 610 nm and 41% at 1300 nm (Figure 5g), and the coloration/bleaching times were 17.5/10.5 s at 610 nm and 18/13 s at 1300 nm, respectively. The CE values at 610 and 1300 nm were 102 and 152 cm<sup>2</sup>  $C^{-1}$ , respectively. This research demonstrates the existence of electrochromic phenomena in COFs and highlights the importance of crystalline structures for the long-term stability of ECDs.

The same research group of Wang et al. prepared a Kagome structure COF film (COF<sub>TPDA-PDA</sub>) with three-state NIR electrochromic properties via the same synthesis method (**Figure 6**a). [25] The  $\pi$ -conjugated COF system consisted of N,N,N,N-tetrakis(4-aminophenyl)-1,4-benzenediamine (TPDA) and terephthalaldehyde (PDA), linked by the imine bonds. The adjacent active units (TPDA) in COF<sub>TPDA-PDA</sub> were closer than the counterparts (TAPA) in the first discovered electrochromic COF, indicating stronger electrochromic properties in NIR. A typical three-electrode system was employed with the electrolyte of 0.1 mol L<sup>-1</sup> NaClO<sub>4</sub>/CH<sub>3</sub>CN solution for the electrochemical and spectroelectrochemical (SEC) experiments. There were two

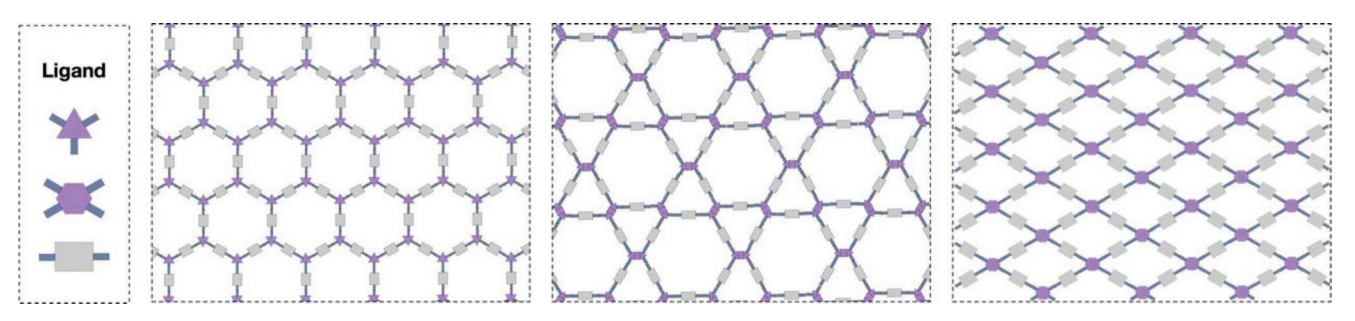


Figure 4. Schematic structures of reported 2D electrochromic COFs, consisting of various organic ligands as building blocks.

2365709x, 2023, 4, Downloaded

onlinelibrary.wiley.com/doi/10.1002/admt.202200917 by University Town Of Shenzhen, Wiley Online Library on [23/11/2025]. See the Terms and Conditions (https://original.com/doi/10.1002/admt.202200917 by University Town Of Shenzhen, Wiley Online Library on [23/11/2025]. See the Terms and Conditions (https://original.com/doi/10.1002/admt.202200917 by University Town Of Shenzhen, Wiley Online Library on [23/11/2025]. See the Terms and Conditions (https://original.com/doi/10.1002/admt.202200917 by University Town Of Shenzhen, Wiley Online Library on [23/11/2025]. See the Terms and Conditions (https://original.com/doi/10.1002/admt.202200917 by University Town Of Shenzhen, Wiley Online Library on [23/11/2025]. See the Terms and Conditions (https://original.com/doi/10.1002/admt.202200917 by University Town Of Shenzhen, Wiley Online Library on [23/11/2025].

and-conditions) on Wiley Online Library for rules of use; OA articles are governed by the applicable Creative Commons License

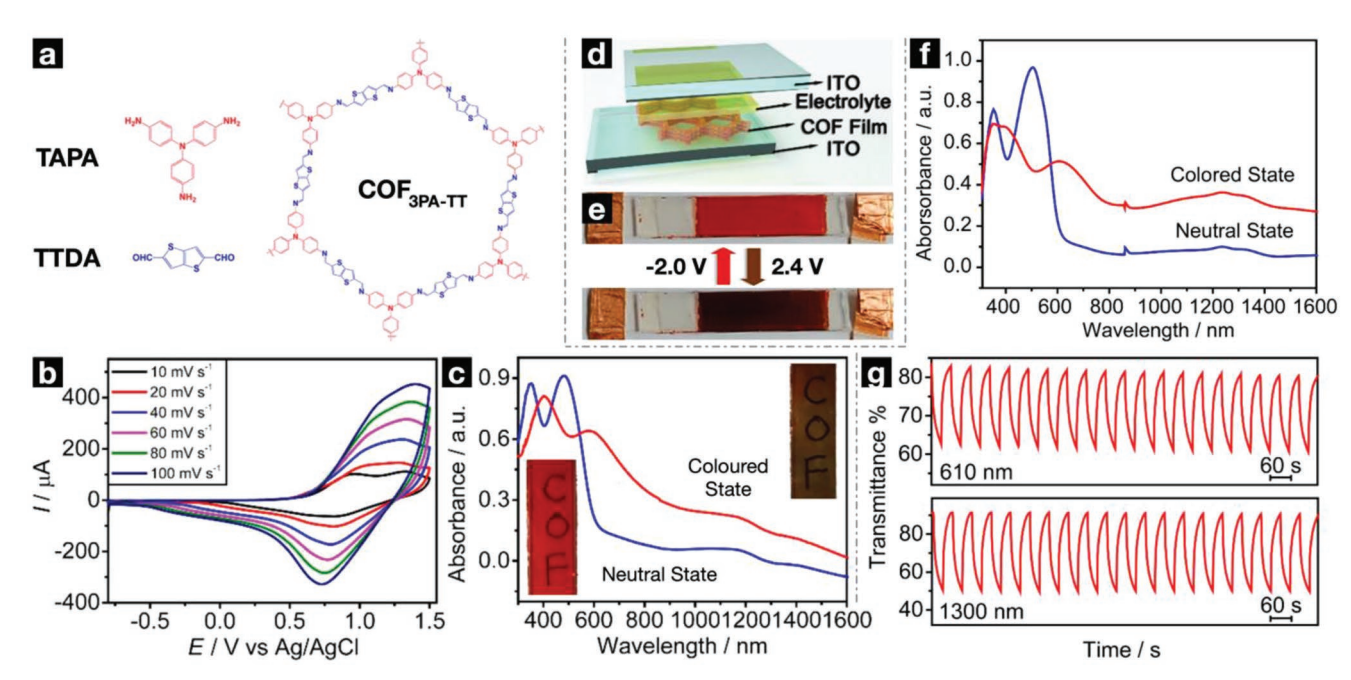


Figure 5. The structure and electrochromic performance of COF<sub>3PA-TT</sub>: a) chemical structures of TAPA, TTDA, and COF<sub>3PA-TT</sub>; b) CV curves of the COF<sub>3PA-TT</sub> film on ITO with the electrolyte of 0.1 mol L<sup>-1</sup> LiClO<sub>4</sub>/PC solution; c) absorbance spectra of the COF<sub>3PA-TT</sub> film on ITO at 0 (blue) and 1.4 V (red), with corresponding photographs showing color changes; d) the structural diagram of the fabricated ECD based on the COF<sub>3PA-TT</sub> film; e) photographs of the ECD under the potential of -2.0 and 2.4 V; f) absorbance spectra of the fabricated ECD at -2.0 (neutral) and 2.4 V (colored); g) transmittance versus time at 610 nm (up) and 1300 nm (down) during 20 cycles under the cyclic voltage between -2.0 and +2.4 V. Adapted with permission. [16] Copyright 2019, American Chemical Society.

obvious redox peaks in the CV curves at about 0.40-0.65 V and 0.80-0.95 V, respectively (Figure 6b), accompanied by reversible three color states (plum, grey, and light blue). As shown in the SEC spectra in Figure 6c, the COF<sub>TPDA-PDA</sub> film had an intense absorption peak at around 486 nm at 0 V, which decreased under step-wisely applied potential from +0.30 to +0.75 V, accompanied by gradually increasing peaks at 400 and 600 nm as well as the NIR region around 1000 nm. These changes in absorbance originated from the partially oxidized TPA units. The induced cation radicals formed a mixed-valence system with adjacent unoxidized ones, resulting in a strong electronic coupling effect and IVCT absorption at around 1000 nm. While raising the potential from +0.75 to +0.90 V (Figure 6d), a new peak emerged at 740 nm with decreasing absorption band in the NIR region, corresponding to the further oxidation process of TPA, in which a large amount of induced TPA cations broke the mixed-valence systems. The optical contrast of the COF<sub>TPDA-PDA</sub> film was 52% at 1050 nm via double-potential-step chronoamperometry (-0.20 V and +0.75 V vs Ag/AgCl) experiments. Corresponding 90% response times for coloring and bleaching were 1.3 and 0.7 s, with the CE value of 320 cm<sup>2</sup> C<sup>-1</sup>. Meanwhile, the COF<sub>TPDA-PDA</sub> film still performed well with obvious redox peaks after 1000 cycles, benefiting from intralayer delocalized electrons and interlayer  $\pi$ - $\pi$  interactions. The memory effect was excellent, with retention time at 1050 nm for more than 2 h, so a prototype of a flip-flop logic gate with memory function was developed based on electrochromic COF<sub>TPDA-PDA</sub> film in the NIR region (Figure 6e,f). By applying voltages of +0.75 V or +0.90 V, an "erase" or "write" operation was conducted, respectively (Figure 6g). The output results can be "read" by monitoring the absorption coefficients at 740 and 1150 nm under no applied potential. Thus, a flip-flop memory system could perform through "write-read-erase-read" cycles (Figure 6h), with the ON/OFF ratio for two output signals being 3.0 and 1.7, respectively, further broadening the application areas of the COF<sub>TPDA-PDA</sub> film. This electrochromic COF film, with three states and sub-second response times in the NIR region, indicates the enormous potential of the development of electrochromic COF materials and extensive applications in electronic and optoelectronic devices.

Zhang et al. [26] adopted the donor-acceptor strategy to construct an extended delocalized  $\pi$ -electron EC-COF-1, with the building blocks of donor N,N,N',N'-tetrakis(p-aminophenyl)-pbenzenediamine (TPBD) and acceptor 2,1,3-benzothiadiazole-4,7-dicarboxaldehyde (BTDD) (Figure 7a,b). The EC-COF-1 film was deposited on ITO electrodes through the solvothermal polycondensation reaction with a thickness of 500  $\pm$  20 nm. A quasi-solid-state device was fabricated where the EC-COF-1 filmdeposited ITO glass was used as the working electrode, another blank ITO glass as the counter electrode, with a quasi-solid electrolyte of LiClO<sub>4</sub>/PC-based polymethyl methacrylate (PMMA) polymer gel. The in situ absorbance spectra of the device under the applied voltage of 0.0-2.0 V are shown in Figure 7c. At 0.0 V, the neutral state EC-COF-1 film displayed a blue-purple color with absorption peaks at 370 and 574 nm. As raising the applied voltages to +2.0 V, the oxidation processes led to the diminishing of these two peaks until fully replaced by new peaks at 730 nm in the visible region and 1400 nm in the NIR region, with color changed to transparent. Corresponding optical contrast ( $\Delta T\%$ ) was 33% at 574 nm and 12%

2365709x, 2023, 4, Downloaded from https://advanced.onlinelibrary.wiley.com/doi/10.1002/admt.202200917 by University Town Of Shenzhen, Wiley Online Library on [23/11/2025]. See the Terms and Condition

on Wiley Online Library for rules of use; OA articles are governed by the applicable Creative Commons License

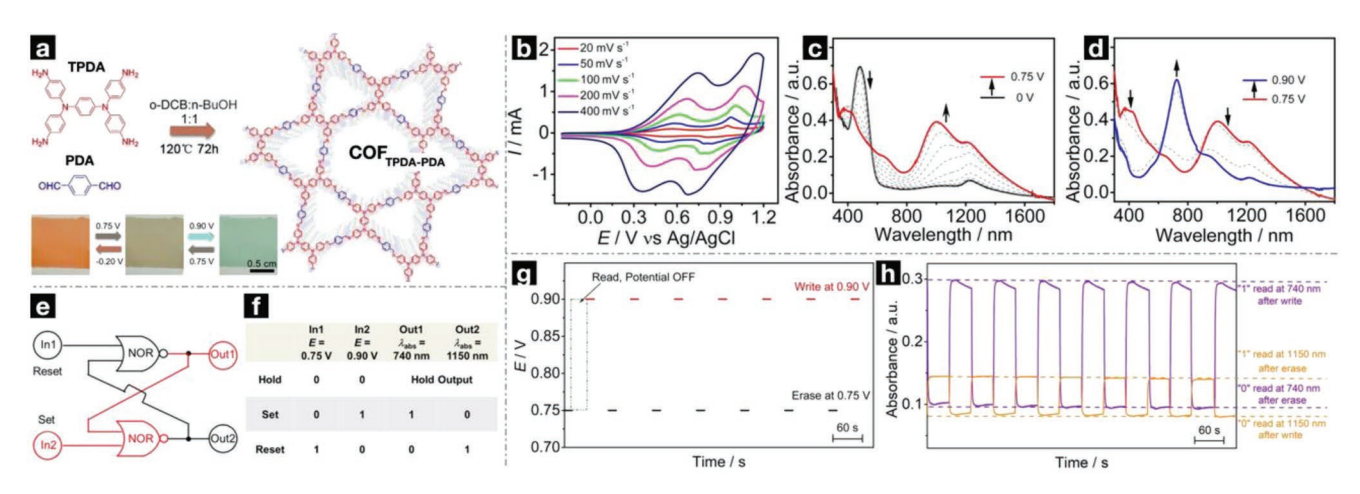


Figure 6. The structure, electrochromic performance, and application of  $COF_{TPDA.PDA}$ : a) chemical structures of TPDA, PDA, and  $COF_{TPDA.PDA}$  with photographs of the  $COF_{TPDA.PDA}$  film at -0.20, 0.75, and 0.90 V in the left bottom; b) CV curves of the  $COF_{TPDA.PDA}$  film in 0.1 mol  $L^{-1}$  NaClO<sub>4</sub>/CH<sub>3</sub>CN solution; Absorbance spectra of the  $COF_{TPDA.PDA}$  film under the applied voltage of c) 0–0.75 V and d) 0.75–0.90 V; e) the logic circuit and f) truth table of the flip-flop logic gate device; g) the applied potential versus time for "write" and "erase" operations; h) absorbance of the  $COF_{TPDA.PDA}$  film at 740 and 1150 nm as output signals. Adopted with permission. [25] Copyright 2021, John Wiley and Sons.

at 730 nm, which dropped only  $\approx$ 0.3% at 574 nm and 0.5% at 730 nm after 15 cycles of switching potential between -1.8 and +2.0 V (Figure 7d). The 90% response times for coloring and bleaching were 1.8/7.2 s at 574 nm and 2.6/3.5 s at 730 nm,

respectively, with the CE values of 284 cm<sup>2</sup> C<sup>-1</sup> at 574 nm and 246 cm<sup>2</sup> C<sup>-1</sup> at 730 nm. The EC-COF-1 film had good cycling stability with minimal changes in the CV curves after 200 cycles (Figure 7e). Computational tools were employed to further

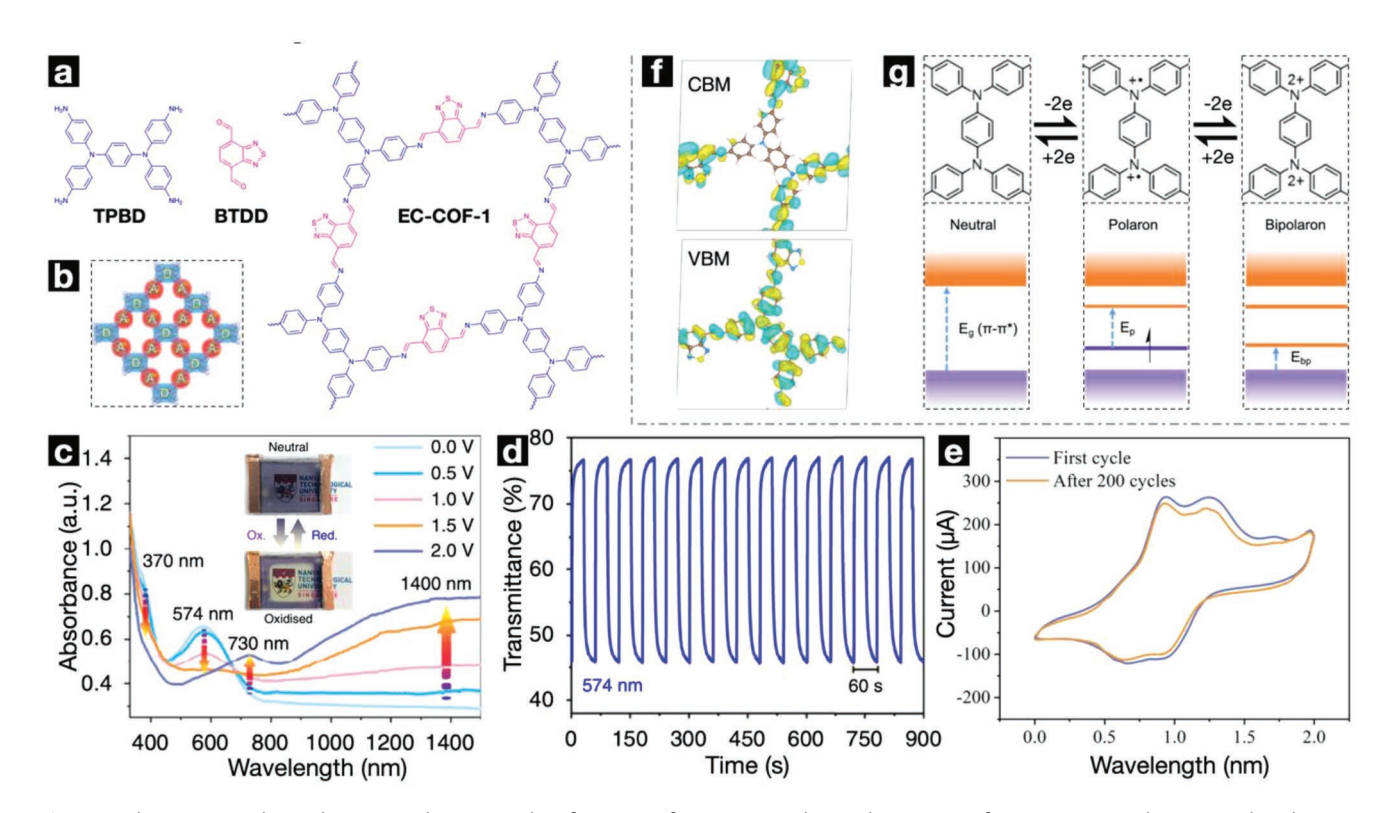


Figure 7. The structure, electrochromic mechanism, and performance of EC-COF-1: a) chemical structures of TPBD, BTDD, and EC-COF-1; b) schematic diagram of the donor–acceptor structure in EC-COF-1; c) absorbance spectra under applied voltage from 0.0 to 2.0 V, with photographs showing the color changes of EC-COF-1 film at neutral and oxidized states; d) transmittance versus time at 574 nm under cyclic voltage between –1.8 and +2.0 V for 15 cycles; e) CV curves of the EC-COF-1 film in the first and 200th cycles; f) HOMO and LUMO for the EC-COF-1 at the neutral state; g) schematic illustration of charge transfer processes with corresponding changes in band structure in EC-COF-1. Adapted with permission. [26] Copyright 2020, Springer Nature.

of use; OA articles are governed by the applicable Creative Commons

ADVANCED MATERIALS

www.advancedsciencenews.com www.advmattechnol.de

study the electrochromic mechanism of the EC-COF-1 film where the pristine EC-COF-1 is a semiconductor with an indirect bandgap of 0.64 eV, in good consistence with the experimental value of 0.75 eV. The highest occupied molecular orbital (HOMO) was mainly located on the TPBD donor unit. In contrast, the lowest unoccupied molecular orbital (LUMO) was delocalized on the BTDD acceptor units (Figure 7f), indicating good  $\pi$ -conjugation. Meanwhile, the atomic orbitals of C and N dominated in the HOMO and LUMO according to the partial density of states, confirming the expanded  $\pi$ -conjugated feature. The applied voltages initially induced a two-electron oxidation process, resulting in polaron species (Figure 7g). With the rising of applied voltages, polarons became bipolarons, which further reduced the bandgap and enhanced the absorption coefficient in the NIR region. This study successfully utilizes the donor-acceptor strategy in electrochromism and points out ways for improving optical contrast.

To systematically investigate the donor-acceptor design strategy, Bein et al.[27] fabricated several COFs based on pyrene tetraaniline (Py(NH<sub>2</sub>)<sub>4</sub>) (Figure 8a) with different bridging units, including electron-rich units of thienothiophene (TT, donor) and naphthalene (N, donor), electron-deficient units of thienoisoindigo (TII, acceptor), and combination units of ttTII and nTII (Figure 8b). The synthesized COF films were grown on ITO glass (Py-ttTII, Py-TT, Py-TII, and Py-N) or 10 nm Au on glass (Py-nTII) substrates via modified solvothermal methods. These COF thin film-deposited electrodes were employed as the working electrodes in typical three-electrode systems, with the counter and reference electrodes of a Pt wire and Ag/AgCl, respectively. The electrochromic behavior was investigated in 0.1 mol L<sup>-1</sup> tetrabutylammonium hexafluorophosphate (TBAPF<sub>6</sub>)/CH<sub>3</sub>CN solution. Py-ttTII (Figure 8c) had symmetrical CV curves on the upper and lower side that the corresponding oxidation and reduction peaks were shifted by only around 20 mV, indicating excellent reversibility of the redox reaction and fast electron transfer kinetics in the

COF, which was further confirmed in the following repeated cycles. During the applied voltage rising from -0.7 to 0.5 V with intervals of 0.2 V, the color of Pv-ttTII changed from dark green to black. And in the corresponding absorption spectra, two absorption peaks of the neutral COF at around 460 and 660 nm gradually diminished, accompanied by new peaks at about 550 and 1000 nm and a large amount of induced radical cations (ttTII+) in the first oxidation step (-0.1 to 0.1 V). The 1000 nm peak shifted to 900 nm after the second oxidation step (0.1–0.3 V), due to the further oxidized dicationic species (ttTII<sup>2+</sup>). The absorption peaks in the range of 330-500 nm originated from the  $\pi$ - $\pi$ <sup> $\star$ </sup> transitions, while the others in the wavelengths longer than 500 nm could be attributed to ICT between donor and acceptor units. The absorption peak at 1000 and 900 nm corresponded to the ttTII+ and ttTII<sup>2+</sup> species, respectively. The response speed of Py-ttTII was the fastest among electrochromic COFs, outcompeting other COFs and typical WO3 by over an order of magnitude. The coloration and bleaching times were 0.38 and 0.2 s at 550 nm, respectively. Meanwhile, the Py-ttTII COF can maintain 95% of its optical contrast after 100 cycles and 85% after 200 cycles. The values of CE were as high as 318 cm $^2$  C $^{-1}$  at 550 nm, 620 cm $^2$  C $^{-1}$  at 660 nm, and 858 cm<sup>2</sup> C<sup>-1</sup> at 880 nm, respectively. While for Py-TII (Figure 8d) and Py-TT (Figure 8e) under the voltage range of -0.7 to 0.7 V, the colors changed from light green to transparent and orange to olive green, respectively. The peak shifting phenomenon was not observed in Py-TII and Py-TT COF, indicating that ICT-induced intense absorption only existed in COFs with donor-acceptor structures. And Py-TII and Py-TT were less stable in electrochemical cycling processes that noticeable changes appeared after the tenth consecutive cycling, which might come from the smaller pore size that hindered ions diffusion in the electrolyte. The Py-TII, Py-TT, and Py-N (Figure 8f) COFs require larger positive potentials (+0.7 V) for oxidation, and the redox peaks in CV curves of PynTII (Figure 8g) were not apparent with poor changes in color.

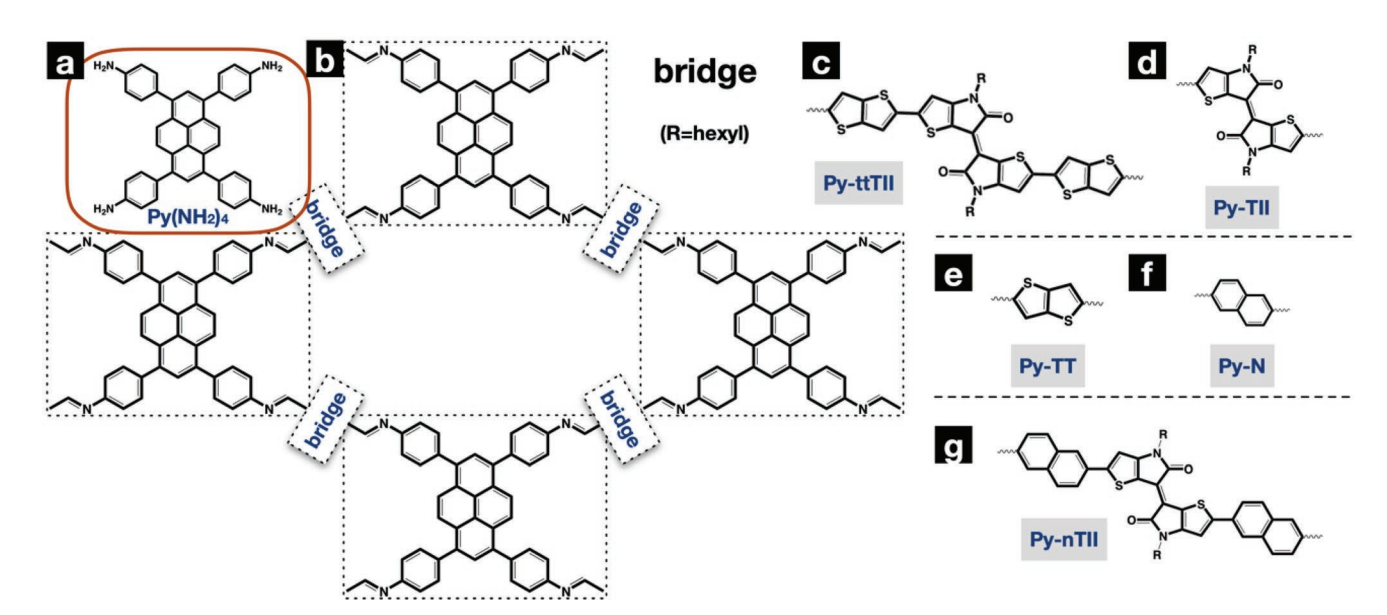


Figure 8. The chemical structure of pyrene tetraaniline (a) and constructed COFs (b) via co-condensation with bridging units (c-g) in ref. [27].

2365709x, 2023, 4, Downloaded from https://alvanced.onlinelibrary.wiley.com/doi/10.1002/admt.202200917 by University Town Of Shenzhen, Wiley Online Library on [23/11/2025]. See the Terms and Conditions (https://onlinelibrary.wiley.com/term

and-conditions) on Wiley Online Library for rules of use; OA articles are governed by the applicable Creative Commons License

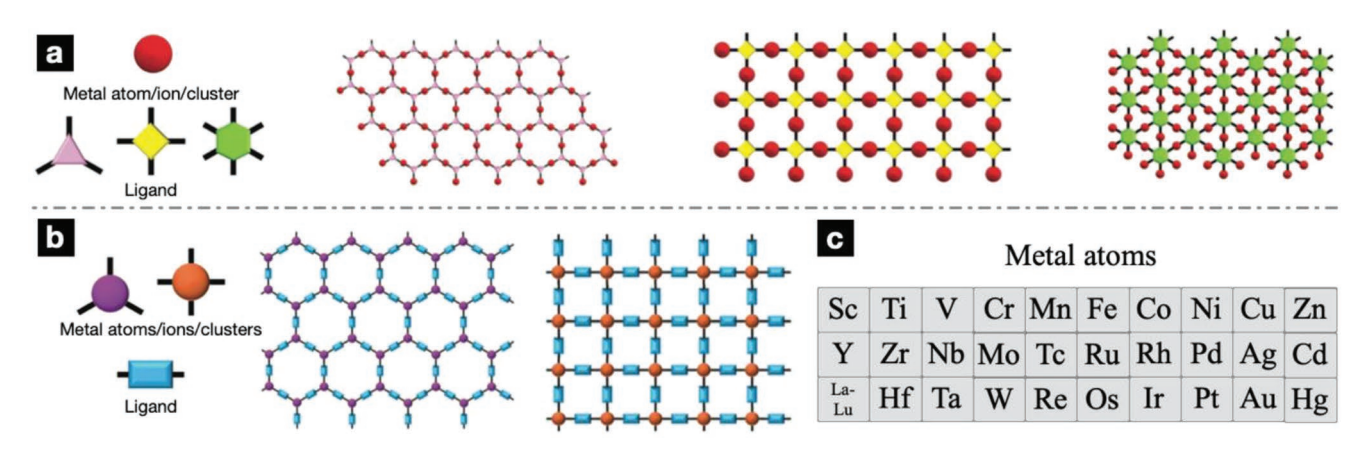


Figure 9. Various combinations of metal atoms/ions/clusters and ligands produce diversified CONASHs with unique physical and chemical properties: a) a metal atom/ion/cluster and organic ligands with three-, four-, and six-fold symmetry; b) metal atoms/ions/clusters with three- and four-fold symmetry and a linear organic ligand. c) Possible metal atoms in CONASHs. a,b) Adapted with permission. [28] Copyright 2017, Royal Society of Chemistry.

This study provides detailed insights into the donor-acceptor strategy, which promotes the future design of COFs with improved electrochromic performance.

So far, there are only four papers reporting the electrochromic effect in 2D COFs, which are generally synthesized via solvothermal polycondensation methods and investigated on transparent ITO glass in typical three-electrode systems. These COFs have intralayer  $\pi$ -conjugated and interlayer  $\pi$ - $\pi$ stacking structures, resulting in good electron conductivity and crystallinity, respectively. The oriented pore structures of COFs can form 1D diffusion channels for ions in electrolytes, improving the electrochemical and electrochromic performance. In terms of COF design, a mixed-valence system can lead to strong absorption in the NIR region, while the donor-acceptor strategy performs well from the visible to the NIR with increased sensitivity of the absorption spectra toward electrochemical oxidation. These two approaches, and others yet to be discovered, will provide guidelines for improving the electrochromic performance of 2D COFs in future research.

#### 3.2. CONASHs

CONASHs, a group of emerging 2D materials, consist of metal ions and organic ligands via coordination bonds and can be synthesized via top-down and bottom-up methods.<sup>[28]</sup> Since 2003, consecutive research has been reported about the structures and characteristics of CONASHs, [29-34] and the research focus switched to the structure-induced unique physical and chemical properties in 2013.[35] A wide range of applications has been proposed mainly by Nishihara and co-workers for CONASHs, such as topological insulators, [36] catalysts for oxygen reduction reaction<sup>[37]</sup> and hydrogen evolution reaction (HER),<sup>[38]</sup> energy storage devices,[39] and photoelectric conversion systems,[40] as well as electrochromism first reported in 2015.[13] By choosing different ligands and metal ions, a series of electrochromic CONASHs have been fabricated with distinct electrochemical and electrochromic performance, discussed in detail in this section (Figure 9).

Nishihara et al. [13] synthesized  $\pi$ -conjugated nanosheets from terpyridine ligands 1,3,5-tris(4-(2,2':6",2"-terpyridyl)phenyl)benzene (1) or 1,3,5-tris((2,2':6',2"-terpyridyl)ethynyl)-benzene (2) and iron (II)/cobalt (II) (Figure 10a) at the interface of aqueous and organic solutions, named as 1-Fe (Figure 10b), 2-Fe (Figure 10c), and 1-Co (Figure 10d), respectively, with a flat and smooth morphology. The solutions for 1-Fe/2-Fe are aqueous Fe(BF<sub>4</sub>)<sub>2</sub> and dichloromethane (CH<sub>2</sub>Cl<sub>2</sub>), while aqueous CoCl<sub>2</sub> and chloroform (CHCl<sub>3</sub>) for 1-Co. The thicknesses of 1-Fe/2-Fe and 1-Co are ≈200 nm/180 nm (corresponding to ≈140/130 layers) and 120 nm (≈90 layers), respectively, which could be adjusted by altering reaction conditions, such as the ion concentrations in the aqueous solutions and reaction time. For example, in dilute aqueous  $Fe(BF_4)_2$  solution (5 mmol  $L^{-1}$ ), the thickness of prepared 1-Fe would be 9-10 nm (six to seven layers) with a reaction time of 1 day, and 180 nm (≈130 layers) with a reaction time of 5 days. Similarly, 1-Co would be 120 nm thick when using 50 mmol L-1 aqueous CoCl2 for 8 days and 10 nm thick with 25 mmol L<sup>-1</sup> aqueous CoCl<sub>2</sub> for 1 day. Through the CV analysis, pristine 1-Fe deposited on the ITO glass had an isolated absorption peak in the visible region at 578 nm and a deep purple color (Figure 10b) due to the metal-to-ligand charge transfer (MLCT). When applying a voltage of 1.16 V, 1-Fe was oxidized to pale yellow, and the previous absorption peak disappeared, which would emerge again with the original color back after being reduced at 0.16 V. The response time and durability of 1-Fe were obtained via potential-step chronoamperometry, namely 0.35 s and over 800 cycles, respectively. For 2-Fe, the color changed from deep violet to pale yellow at 1.27 V and back to the original at 0.27 V (Figure 10c). The absorption peak at 588 nm diminished when oxidized and revived after reduction. The response time is 0.54 s with good durability of over 1000 cycles. Unlike 1-Fe and 2-Fe, there are two redox pairs for 1-Co, Co<sup>3+</sup>/Co<sup>2+</sup> and Co<sup>2+</sup>/Co<sup>+</sup>. Due to the slow electron transfer rate of Co3+/Co2+ shown in CV results, only electrochromic performance corresponding to Co<sup>2+</sup>/Co<sup>+</sup> was studied. The pristine 1-Co was orange and could be reduced to a deep purple at -1.35 V (Figure 10d), resulting in an enhanced absorption coefficient with a peak at ≈600 nm. Solid-state electrochromic systems were fabricated to simulate practical applications. The

2365709x, 2023, 4, Downloaded

onlinelibrary.wiley.com/doi/10.1002/admt.202200917 by University Town Of Shenzhen, Wiley Online Library on [23/11/2025]. See the Terms

and-conditions) on Wiley Online Library for rules of use; OA articles are governed by the applicable Creative Commons License

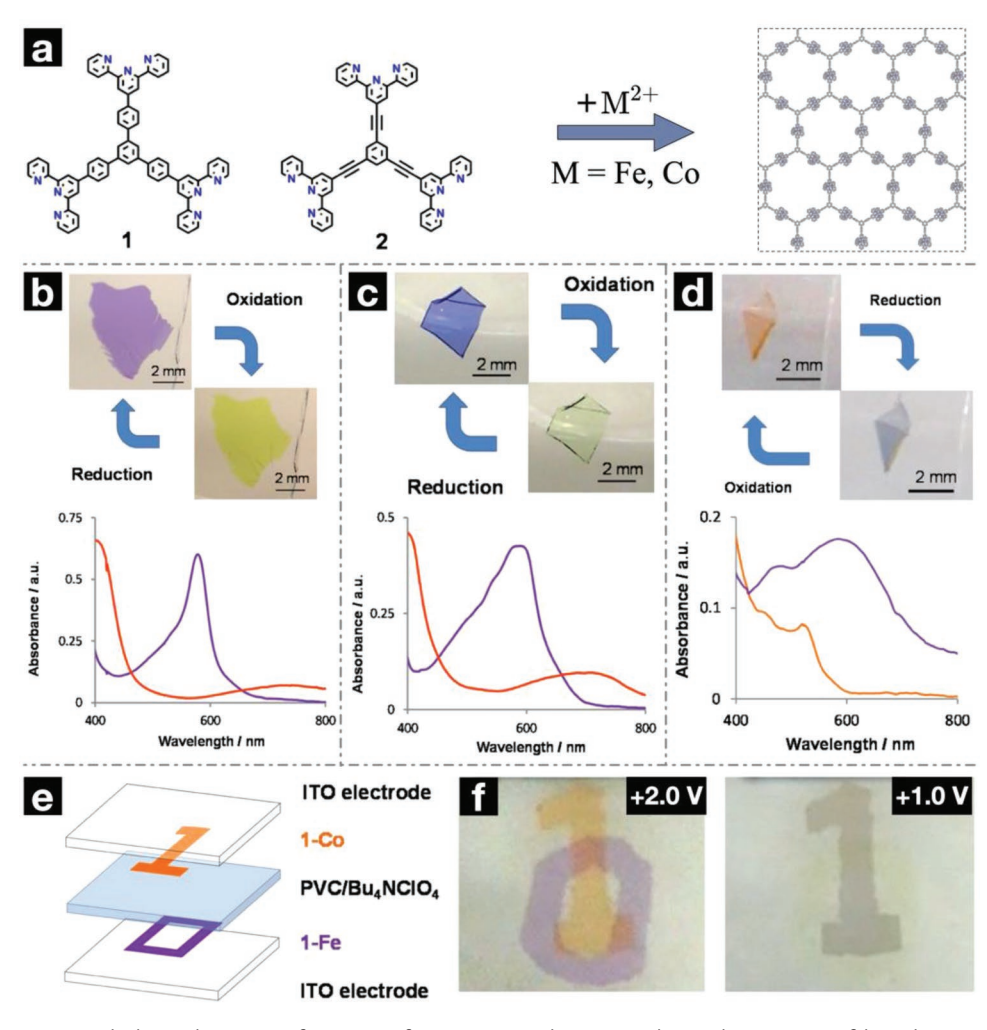


Figure 10. The structures and electrochromic performance of 1-Fe, 2-Fe, and 1-Co: a) chemical structures of ligands 1, 2, and corresponding bis(terpyridine) metal(II) complex nanosheets; electrochromism, and UV-vis spectra of b) 1-Fe, c) 2-Fe, and d) 1-Co, with absorbance curves of pristing and oxidized states in purple and orange, respectively; e) schematic structure of dual-ECD made up of 1-Fe and 1-Co; f) digital photographs of the dual-ECD under the voltage of +2.0 and +1.0 V. Adapted with permission. [13] Copyright 2015, American Chemical Society.

ECD with 1-Fe had a reversible color change between deep purple and pale yellow in the voltage range from +3.0 to -1.8 V, with the absorption peak of the initial state at 579 nm. Similarly, 1-Co with orange color was reduced to a deep purple at -4.5 V and recovered at 0 V. Moreover, a hybrid device containing 1-Fe as the working electrode and 1-Co as the counter electrode showed "dual" electrochromism was prepared, with corresponding structures shown in Figure 10e. 1-Fe and 1-Co were in the shapes of "0" and "1," respectively, and performed electrochemical reactions simultaneously. By applying voltages between +2.0 and +1.0 V, the hybrid device highlighted "0" and "1" alternately (Figure 10f). This work opened the world of electrochromism in CONASHs.

Higuchi et al.[41] successfully prepared two CONASHs (NBP1 and NBP2) with new molecular structures, consisting bis(2,2'-bipyridine) derivatives (BP1 and BP2) as coordination ligands and Fe2+ as coordinating metal ions (Figure 11a). The ligands (10<sup>-4</sup> mol L<sup>-1</sup>) are dissolved in CH<sub>2</sub>Cl<sub>2</sub> as the bottom layer, with  $Fe(BF_4)_2 \cdot 6H_2O$  (10<sup>-2</sup> mol L<sup>-1</sup>) aqueous solution as the top layer. After keeping the system for 24 h, blue and

magenta color films of NBP1 and NBP2 were generated at the interface (Figure 11b). The color difference originated from the spacer in the ligands. For NBP1, there were three peaks in the absorbance curves, namely 317, 412, and 590 nm. The first peak (317 nm) corresponded to  $\pi$ – $\pi$ \* transitions, while the latter two can be attributed to the MLCT mechanism  $(d-\pi^*)$  transitions). The absorbance peaks for NBP2 were 298, 378, and 568 nm, with the same transitions as NBP1. The thickness for NBP1 and NBP2 was 165 nm (≈66 layers) and 200 nm (≈80 layers), respectively. By adopting the Langmuir-Blodgett system, monolayer NBP1 was synthesized at an air-water interface, with the average thickness of 2.4 nm measured via atomic force microscopy. CV analysis and electrochromic performance were conducted in a three-electrode electrochemical system, with CONASHs-deposited ITO as the working electrode, a platinum flag as the counter electrode, Ag/AgCl as the reference electrode, and 0.1 mol L-1 LiClO<sub>4</sub>/CH<sub>3</sub>CN as the electrolyte. Reversible redox peaks of the Fe<sup>2+</sup>/Fe<sup>3+</sup> pair were observed at a scan rate of 50 mV s<sup>-1</sup>, with half-wave potentials of 0.68 and 0.61 V for NBP1 and NBP2, respectively. Through the SEC

2365709x, 2023, 4, Downloaded from https

onlinelibrary.wiley.com/doi/10.1002/admt.202200917 by University Town Of Shenzhen, Wiley Online Library on [23/11/2025]. See the Terms and Conditions (https://onlinelibrary.wiley.com/term

and-conditions) on Wiley Online Library for rules of use; OA articles are governed by the applicable Creative Commons License

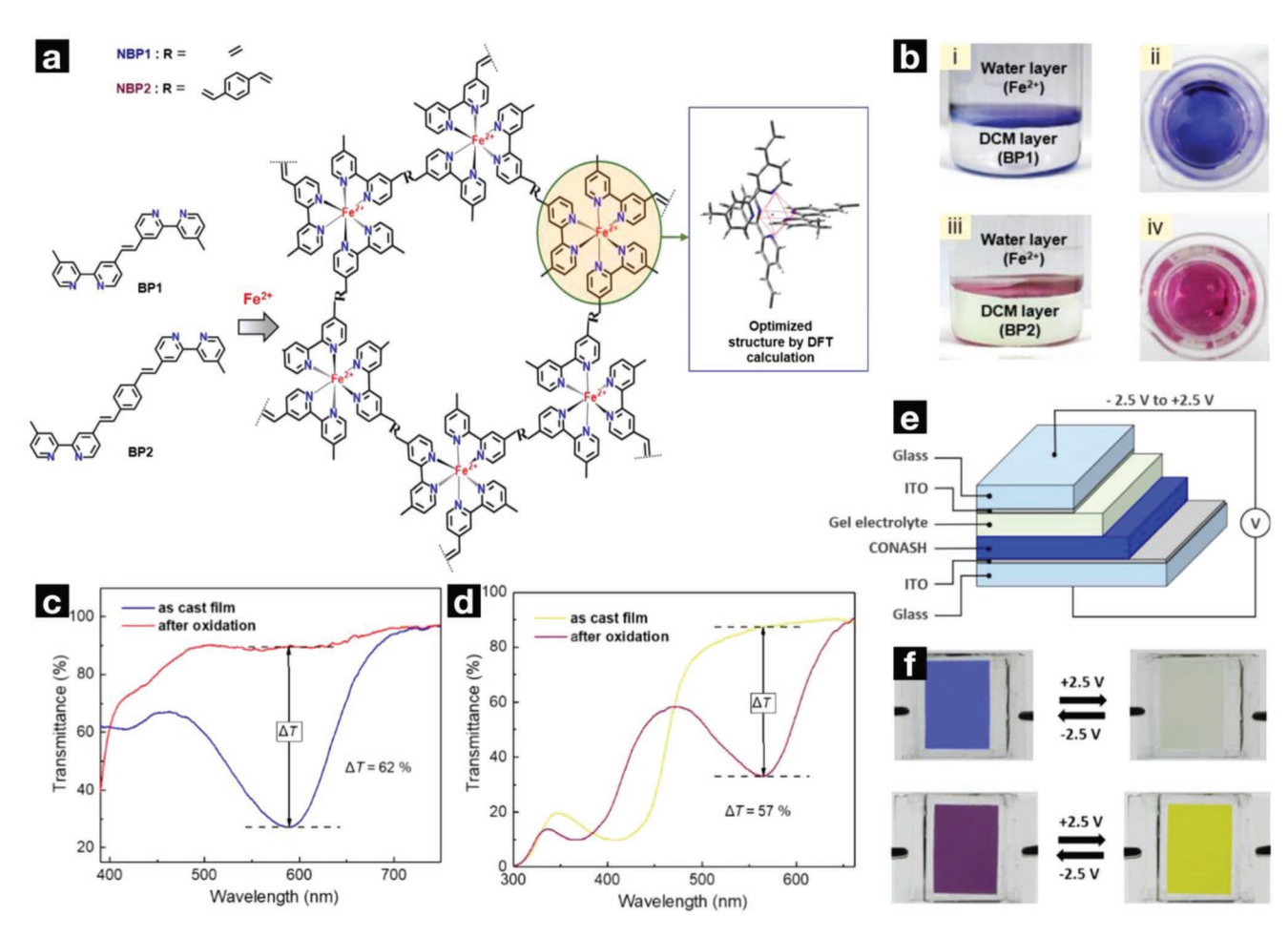


Figure 11. The structure, synthesis, and electrochromic performance of two CONASHs (NBP1 and NBP2): a) chemical structures of the BP1, BP2 ligands, and corresponding CONASHs, with the inset showing the octahedral coordination mode of Fe<sup>2+</sup> obtained via density functional theory (DFT) calculations; b) side and top view of synthesized NBP1 (i, ii) and NBP2 (iii, iv) films in glass beakers; c,d) transmittance spectra of NBP1 films at 590 nm (c) and NBP2 films at 568 nm (d) before and after oxidation; e) schematic structure of the solid-state ECD based on CONASHs; f) digital photographs of the device based on NBP1 (up) and NBP2 (down) before and after oxidation. Adapted with permission. [41] Copyright 2019, American Chemical Society.

measurements in the voltage range of 0-1 V, the optical contrast ( $\Delta T\%$ ) was 62% at 590 nm and 57% at 568 nm for NBP1 and NBP2, respectively (Figure 11c,d). The reversible color changes were between blue and colorless for NBP1 and between magenta and yellow for NBP2. Both CONASHs maintained almost unaltered  $\Delta T$  after 1500 cycles, with the 95% coloration/ bleaching times being 0.48/0.57 s for NBP1 and 0.50/0.54 s for NBP2, respectively. Corresponding CE was calculated to be 431 and 382 cm<sup>2</sup> C<sup>-1</sup>, respectively. Moreover, solid-state ECDs were fabricated with the structure shown in Figure 11e. By applying cyclic voltage in the range from -2.5 to 2.5 V, colors changed from blue to colorless for the NBP1-based device and magenta to yellow for the NBP2-based device (Figure 11f). Corresponding optical contrast ( $\Delta T\%$ ) was 60% and 61%, with coloration/bleaching times being 0.73/1.44 and 1.71/2.5 s for NBP1 and NBP2, respectively. Both devices were stable for over 300 electrochemical processes. The novel building blocks-constructed CONASHs, with excellent cycling stability comparable to some of the best-performing electrochromic materials, are potential electrochromic materials for next-generation display applications.

Wong et al.[42] synthesized two CONASHs Co-S1 and Co-S2 from trifunctional terpyridine-based TPA derivatives (L1 and L2) and Co(BF<sub>4</sub>)<sub>2</sub> · 6H<sub>2</sub>O via liquid-liquid interfaceassisted synthesis, as shown in Figure 12a-c. Both Co-S1 and Co-S2 had good thermostability, tested by thermal gravimetric analysis. The electrochemical properties of Co-S1 and Co-S2 were studied in a three-electrode system where the CONASHs-modified ITO glass was used as the working electrode, and the platinum wire and Ag/AgNO3 were performed as the counter and reference electrodes, respectively, with the electrolyte of 1 mol L<sup>-1</sup> TBAPF<sub>6</sub>/CH<sub>2</sub>Cl<sub>2</sub>. For Co-S1, there are two redox waves at  $E^0 = 1.35$  and 0.3 V in the CV curves (Figure 12d). The former could be attributed to the redox couple of the TPA unit and the TPA radical cation. The latter corresponded to the Co<sup>3+</sup>/Co<sup>2+</sup> couple. For Co-S2, there are two redox peaks at 0.6 and 1.2 V with a scan rate of 0.1 V s<sup>-1</sup> (Figure 12e), corresponding to the TPA/TPA radical cation couple with  $E^0$  of about 0.9 V. By analyzing the relationship between anodic/ cathodic current with the scan rates, these electrochemical reactions were complicated diffusion-controlled processes with good reversibility confirmed by the charge-time response curve.

2365709x, 2023, 4, Downloaded

onlinelibrary.wiley.com/doi/10.1002/admt.202200917 by University Town Of Shenzhen, Wiley Online Library on [23/11/2025]. See the Terms

ınd-conditions) on Wiley Online Library for rules of use; OA articles are governed by the applicable Creative Commons License

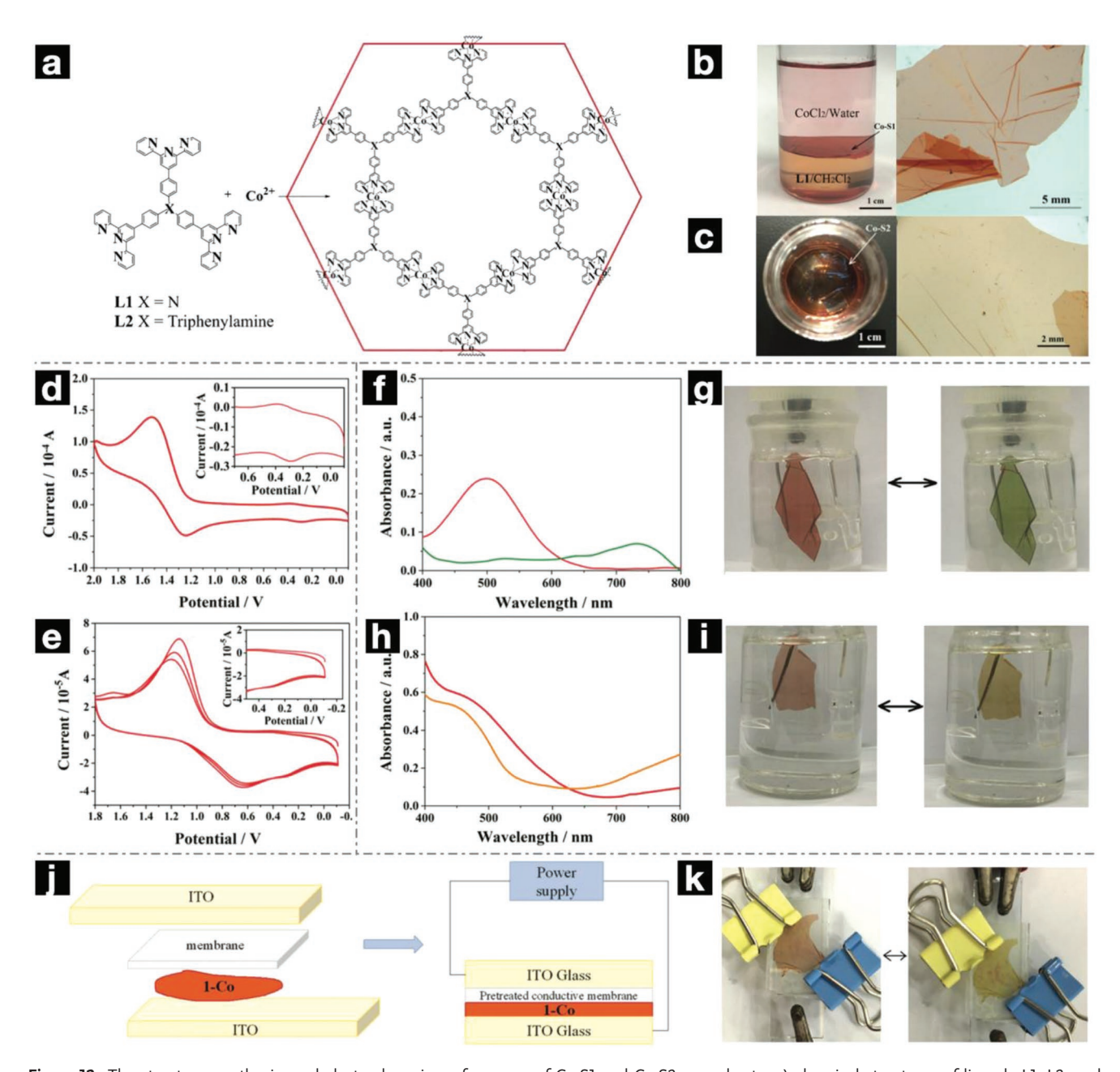


Figure 12. The structure, synthesis, and electrochromic performance of Co-S1 and Co-S2 nanosheets: a) chemical structures of ligands L1, L2, and corresponding Co-S1 and Co-S2 nanosheets; the synthesized b) Co-S1 and c) Co-S2 at the liquid–liquid interface and related optical microscopy images on quartz substrates; the CV curves of d) Co-S1 and e) Co-S2 in 1 mol L $^{-1}$  TBAPF $_6$  (CH $_2$ Cl $_2$  solution) at a scan rate of 0.1 V s $^{-1}$  within the scan range of -0.1 to 2.0 V and -0.1 to 1.8 V, respectively, with the insets showing the magnification of CV curves under small potential windows; the UV–vis spectra of the synthesized f) Co-S1 and h) Co-S2 in the pristine states (red) and oxidized states (green, orange) and corresponding electrochromic behavior of g) Co-S1 and i) Co-S2; j) schematic structure of the ECD based on Co-S1; k) digital photographs of the ECD under the potential of -0.5 V (reduction, left) and 3 V (oxidation, right). Adapted with permission. [42] Copyright 2019, Royal Society of Chemistry.

In terms of the electrochromic properties, Co-S1 had an absorption peak at 500 nm (Figure 12f), corresponding to the d–d\* transition band of Co(II). The red color Co-S1 changed to green at 2.0 V with the absorption peak disappeared and changed back at -0.1 V (Figure 12g). While for Co-S2, the absorption peak at around 500 nm was neglectable (Figure 12h), accompanied by color changing from light red to orange (Figure 12i), which might come from the lower thickness than the thicker Co-S1.

The maximum CE for Co-S1 and Co-S2 was 123.76 cm $^2$  C $^{-1}$  at 500 nm and 91.88 cm $^2$  C $^{-1}$  at 540 nm. An ECD based on Co-S1 was fabricated according to the structure in Figure 12j, showing similar electrochromic behavior in Figure 12k.

Zhang et al. [43] synthesized star-shaped CONASHs at the interface between the organic  $CH_2Cl_2$  solution of TPA-TPY and aqueous  $Fe(BF_4)_2$  (Figure 13a,b). With extending the reaction time from 5 to 8 days, the thickness of the generated

ced.onlinelibrary.wiley.com/doi/10.1002/admt.202200917 by University Town Of Shenzhen, Wiley Online Library on [23/11/2025]. See the Terms and Conditions (https://onlinelibrary.wiley

and-conditions) on Wiley Online Library for rules of use; OA articles are governed by the applicable Creative Commons

www.advmattechnol.de

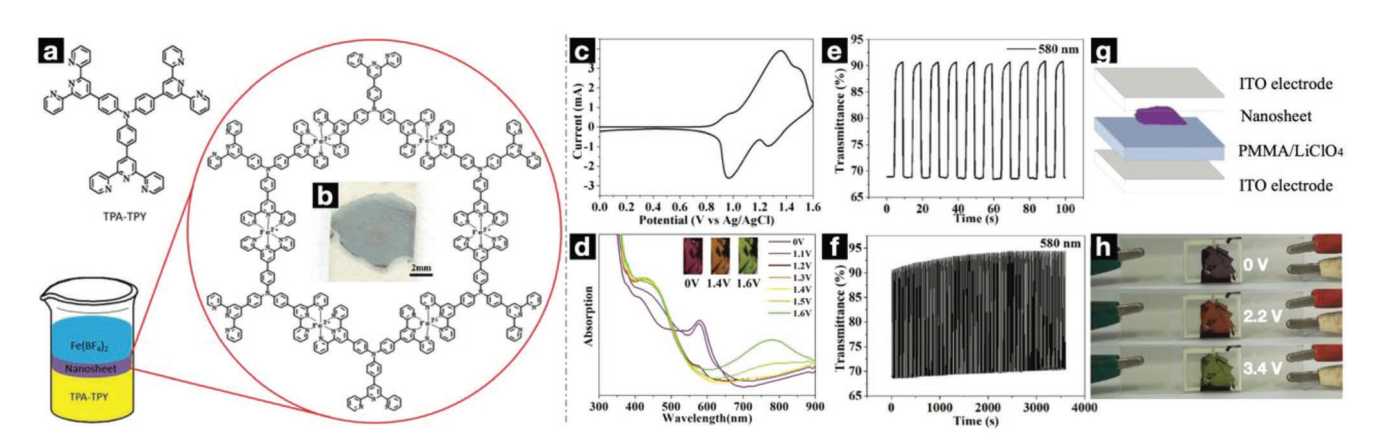


Figure 13. The structure and electrochromic performance of the CONASHs consisted of TPA-TPY ligands and Fe ions: a) chemical structures of ligand tris[4-(4'-2,2':6',2''-terpyridyl)-phenyl]amine (TPA-TPY) and synthesized CONASHs; b) the digital photograph of the CONASHs deposited on an ITO glass; c) CV curve of the CONASHs; d) UV-vis spectra of the CONASHs in 0.1 mol L<sup>-1</sup> CH<sub>3</sub>CN solution of Bu<sub>4</sub>NClO<sub>4</sub>, with insets showing the color of the CONASHs at 0, 1.4, and 1.6 V; e) transmittance versus time at 580 nm under the applied cyclic voltage of 0–1.4 V; f) cycling stability of transmittance at 580 nm for over 3500 s; g) schematic structure of the solid-state ECD; h) digital photographs of the fabricated device under the potential of 0, 2.2, and 3.4 V. Adapted with permission. [43] Copyright 2019, Royal Society of Chemistry.

CONASHs increased from ≈55 nm to about 105 nm. CV analysis (Figure 13c) was performed with the 105 nm thickness CONASHs-deposited ITO glass in 0.1 mol  $L^{-1}$  Bu<sub>4</sub>NClO<sub>4</sub> solution of CH<sub>3</sub>CN. The applied voltage range was 0-1.6 V with a scanning rate of 0.1 V s<sup>-1</sup>. Two oxidation peaks at 1.35 and 1.49 V were observed, with the corresponding reduction peaks at 0.97 and 1.27 V, which should be attributed to the redox behavior of coordinated Fe(II)-terpyridine (1.35/0.97 V) and central TPA group (1.49/1.27 V). The two redox processes generally led to multi-color electrochromism. The electrochromic properties were investigated in a 0.1 mol L<sup>-1</sup> TBAPF<sub>6</sub>/CH<sub>3</sub>CN solution. The pristine CONASHs had a purplish red color with an absorption peak at 580 nm (Figure 13d). As the applied voltage raised from 0 to 1.4 V, the absorption peak at 580 nm was gradually replaced by the peak at 421 nm, with a color change from purplish red to orange-yellow. Under higher voltage at 1.4-1.6 V, a new peak at ≈780 nm emerged, resulting in color changing from orangevellow to green. However, the green color state was unstable and would disappear after several cycles. Under the voltage range of 0–1.4 V, the optical contrast ( $\Delta T\%$ ) at 580 nm and the CE value was 22.3% and 141.72 cm<sup>2</sup> C<sup>-1</sup>, respectively (Figure 13e), with the 95% coloring and discoloring times being 0.5 and 0.4 s, respectively. A series of CONASHs with different thicknesses were tested and found that the switching time was independent of the thickness, while the CE increased with the thickness. The cycling stability was tested for over 500 cycles with almost undiminished optical contrast (Figure 13f). Moreover, a solid-state ECD (Figure 13g) was fabricated with PMMA and LiClO<sub>4</sub> as the solidified electrolyte. The CONASHs-modified ITO glass functioned as the working electrode and one blank ITO as the counter electrode. Under applied voltages, the color of the ECD changed from purplish red to orange-yellow (0-2.2 V) and green (2.2–3.4 V) in Figure 13h. The higher operating voltages than in liquid state electrolytes originated from the relatively low electron conductivity and ions diffusion rates. The coloring and discoloring times were about 1 and 0.9 s, respectively. This research demonstrates that the multi-color electrochromic effect could be introduced in 2D CONASHs.

Higuchi et al.[44] synthesized dual-branched CONASHs with dense hexagonal Fe(II) via the complexation of the tritopic bidentate ligands (L<sub>3Phn</sub>) and Fe(II) ions in equal proportions verified by titration (Figure 14a), forming an octahedral structure where three phenanthrolines coordinated with Fe(II) in the center (Figure 14b). The CONASHs film formed at the interface between the CH<sub>2</sub>Cl<sub>2</sub> solution of L<sub>3Phn</sub> (0.1 mmol L<sup>-1</sup>) and the aqueous solution of  $Fe(BF_4)_2 \cdot 6H_2O$  (0.1 mmol L<sup>-1</sup>) after 6 h with a uniform thickness of 95  $\pm$  5 nm (Figure 14c). The CV analysis was conducted via a three-electrode system that the ITO-coated film functioned as the working electrode, Pt-wire and non-aqueous Ag/Ag+ as the counter and reference electrodes, respectively, in a 0.1 mol L-1 LiClO<sub>4</sub> electrolyte. During cyclically scanning in the voltage range of 0-1 V, the film showed a reversible color change from intense red to colorless (Figure 14d), with the oxidation and reduction peaks of CV curves at 0.87 and 0.63 V (Figure 14e), respectively, corresponding to the redox couple  $Fe^{2+}/Fe^{3+}$  ( $E_{1/2} = 0.75$  V vs Ag/Ag+), shown in Figure 14f. The average optical contrast ( $\Delta T$ %) was around 55% at 518 nm under a double-step potential (Figure 14g), which depended on the film thickness. The coloration and bleaching times were 2.9 and 3.3 s, respectively, with the CE value of about 230 cm<sup>2</sup> C<sup>-1</sup>. Finally, the electrochromic performance of the film was investigated in a solid-state ECD (Figure 14h), with the cathodically coloring CONASHs-deposited ITO glass as the working electrode, the anodically coloring nickel hexacyanoferrate as the counter electrode, and the mixing of PMMA, PC, and LiClO<sub>4</sub> in CH<sub>3</sub>CN solution as the ion-gel electrolyte. The fabricated solid-state ECD could switch between the colored (0 V) and bleached states (1.5 V), with high optical contrast ( $\Delta T\% > 65\%$  at around 518 nm) and long-term durability of over 15 000 cycles (90% retention of original optical properties), as shown in Figure 14i,j. This study indicates that dual-branched CONASHs are promising electrochromic materials with a service life comparable to inorganic oxides.

Chakraborty et al.<sup>[45]</sup> synthesized hyperbranched CONASHs consisting of a three-arm terpyridine(3tpy)-based ligand and Fe(II) ion via interfacial complexation at the liquid–liquid

2365709x, 2023, 4, Downloaded from https://advanced.onlinelibrary.wiley.com/doi/10.1002/admt.202200917 by University Town Of Shenzhen, Wiley Online Library on [23/11/2025]. See the Terms and Conditions (https://onlinelibrary.wiley.com/term

and-conditions) on Wiley Online Library for rules of use; OA articles are governed by the applicable Creative Commons License

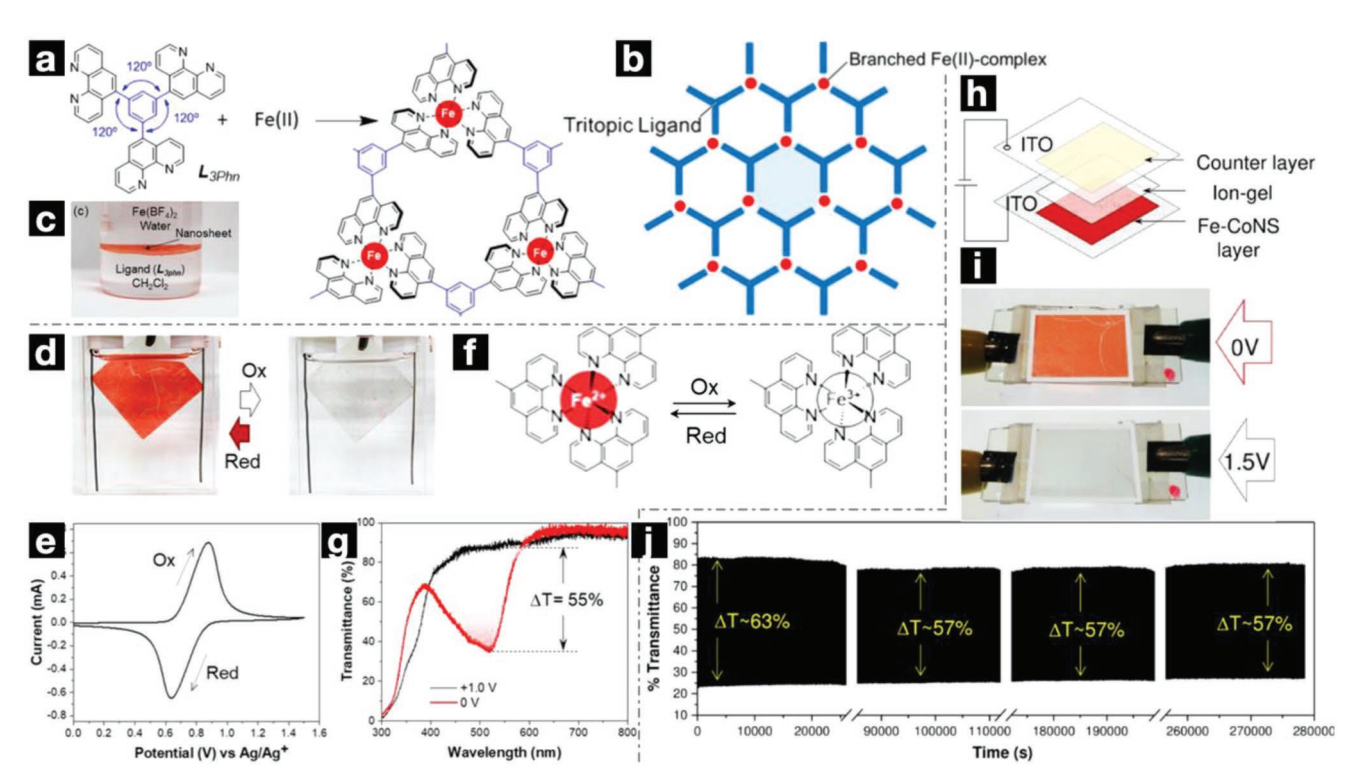


Figure 14. The structures and electrochromic performance of the CONASHs consisted of L<sub>3Phn</sub> ligands and Fe ions: a) chemical structures of ligand 1.3.5-tris (1.10-phenanthrolyl)benzene (Laphn) and synthesized dual-branched CONASHs; b) schematic diagram of CONASHs with a tritopic ligand and branched metal coordination; c) photograph of the synthesized nanosheets at the liquid-liquid interface; d) reversible color change of the CONASHs between intense red (reduced) and colorless states (oxidized); e) CV curve of the film at a scan rate of 50 mV s<sup>-1</sup>; f) redox transformations induced electrochromism; g) transmittance at 518 nm at +1.0 and 0 V for the bleached (black line) and colored (red line) states, respectively; h) schematic structure of the fabricated solid-state ECD; i) digital photographs of the fabricated device under 0 and 1.5 V, respectively; j) long-term stability in transmittance under the potential range of +1.5 to 0 V with a holding time of 15 s for over 15 000 cycles. Adapted with permission [44] Copyright 2020, American Chemical Society.

interface (Figure 15a). The thickness of the 3tpy-Fe CONASHs film was ≈350 nm after 48 h of reaction. The fabricated solidstate ECD based on a 3tpy-Fe film deposited on ITO had an oxidation peak of the Fe<sup>2+</sup>/Fe<sup>3+</sup> couple at around +2 V and a corresponding reduction peak of Fe<sup>3+</sup>/Fe<sup>2+</sup> at about -1.5 V under the voltage range of +3 V to −2 V (Figure 15b). The accompanied color change was from intense pink at -2.0 V to colorless at +3.0 V (Figure 15c). The formed Fe<sup>3+</sup> centers at +3 V led to the reduced peak at 556 nm (Figure 15d), corresponding to the MLCT transition. The peak at 556 nm reappeared at -2 V due to the restoration of Fe<sup>2+</sup> centers, and the optical contrast ( $\Delta T$ ) was 53%. Corresponding 95% coloration and bleaching times were 1.15 and 2.49 s, respectively, with a high CE of 470.16 cm<sup>2</sup> C<sup>-1</sup>. The cycling stability was tested with interval times of 10 s for 1000 cycles and 5 s for 500 cycles. Corresponding decrements were 4.91% and 2.91%, respectively. It was worth noting that the 3tpy-Fe nanosheets exhibited longer electrochromic memory than 2D 3tpyC-Fe nanosheets and 1D polymer of polyFe (Figure 15e), in which the non-conjugated ligand of 3tpy was replaced by conjugated ones. The corresponding chemical structures and photographs showing the decay of the bleached states are presented in Figures 15f and 15g, respectively. The mechanism was attributed to the slow electron transfer from the electrode to all the Fe3+ centers in the 3tpy-Fe film (Figure 15h), induced by the non-conjugated ligand as this characteristic was not observed in the other two conjugated nanosheets. The electrochromic memory is an essential parameter of power efficiency for smart windows, and this research provides further insights into the relationship between ligands and electrochromic properties.

Chakraborty et al.[46] synthesized similar CONASHs using the same three-arm ligand and Co (II), denoted as Cotpy-L (Figure 16a,b), which was investigated in terms of electrochromism in a typical three-electrode system (Figure 16c). By scanning between -1.6 V and 0.8 V in 0.1 mol L-1 KCl/water solution, a reversible redox peak at  $E_{1/2} = -1.1 \text{ V}$  for the Co<sup>2+</sup>/ Co+ redox pair was observed in CV curves, accompanied by color changing between colorless (Co2+) and blackish-green (Co<sup>+</sup>) at 0.0 and -1.4 V, respectively (Figure 16d). The absorption bands of the Co-tpy-L film, due to different transitions in the oxidized and reduced states (Figure 16e), in both aqueous and non-aqueous electrolyte solutions were investigated. The pristine film was transparent with week absorption bands at 453 and 502 nm (Figure 16f), induced by  $d-d^*$  transitions. Three absorption bands appeared under the applied voltage of −1.4 V, with two in the visible region (591 and 419 nm) and one in the NIR region ( $\lambda_{\text{max}} = 1070 \text{ nm}$ ). The band at 591 nm corresponds to the reduction reaction from Co2+ to Co+ in negative potential, while the other two originated from the MLCT

2365709x, 2023, 4, Downloaded from https://advanced.onlinelibrary.wiley.com/doi/10.1002/admt.202200917 by University Town Of Shenzhen, Wiley Online Library on [23/11/2025]. See the Terms and Condition

ons) on Wiley Online Library for rules of use; OA articles are governed by the applicable Creative Commons

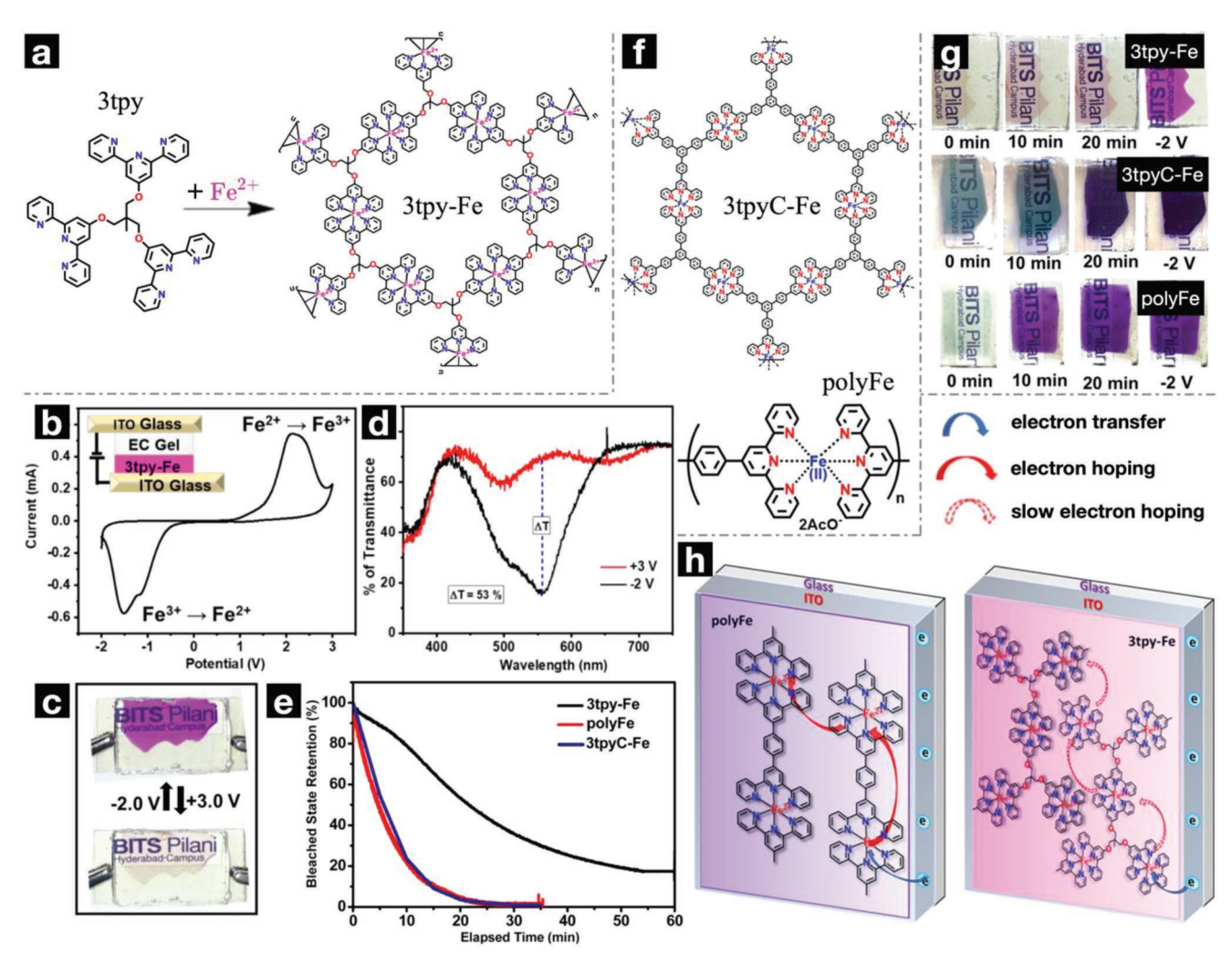


Figure 15. The structures and electrochromic performance of 3tpy-Fe and 3tpyC-Fe CONASHs: a) chemical structures of ligand 3tpy and synthesized 3tpy-Fe nanosheets; b) CV curve of the solid-state ECD based on 3tpy-Fe nanosheets, with an inset showing the schematic structure of the device; c) electrochromic behavior of 3tpy-Fe film at –2.0 and +3.0 V; d) transmittance spectra of the ECD based on 3tpy-Fe nanosheets; e) transmittance decay curves from bleached to colored states for 3tpy-Fe, polyFe, and 3tpyC-Fe films; f) chemical structures of 3tpyC-Fe and polyFe films; g) photographs of the bleached ECDs based on 3tpy-Fe, 3tpyC-Fe, and polyFe films at different times under open-circuit conditions; h) schematic diagram of the proposed mechanism for fast transmittance decay in 1D polyFe and 2D 3tpyC-Fe films. Adapted with permission. [45] Copyright 2020, American Chemical Society.

transitions from electron-rich Co+  $d\pi$  (t\_{2g} and e\_g) to the  $\pi^{\!\star}$ orbital of the electron-acceptor terpyridyl ligand. The Co-tpy-L film could obtain its original color when raising the voltage to 0 V, resulting in the oxidation process from Co<sup>+</sup> to Co<sup>2+</sup>. The optical contrast ( $\Delta T$ ) was 48.3% at 419 nm, 54.1% at 591 nm, and 61.3% at 1070 nm, with 95% coloration and bleaching times at 1070 nm being 7.9 and 2.8 s (Figure 16g). However, poor electrochemical stability (up to 1500 s) was observed in aqueous KCl media due to the HER at negative potential. In a typical three-electrode system with non-aqueous LiClO<sub>4</sub>/PC electrolyte, similar bands in absorption were observed with slight shift (Figure 16h), with corresponding optical contrast ( $\Delta T$ ) being 57.2%, 58.6%, and 64.6% at wavelengths of 414, 604, and 1090 nm, respectively (Figure 16i). The coloration and bleaching times at 1090 nm were 7.6 and 6.1 s, respectively, with CE being 115.8 and 211 cm<sup>2</sup> C<sup>-1</sup> in aqueous KCl

and non-aqueous LiClO<sub>4</sub>/PC electrolytes, respectively. This work extends the electrochromic effect in CONASHs from the visible region to the infrared region, showing the potential of CONASHs in more extensive applications.

All papers on electrochromic CONASHs have been summarized at length in this section. These films of CONASHs are synthesized at the interface of aqueous and organic solutions via coordination polymerization processes. The electrochromic mechanism is mainly due to the MLCT and redox reactions of multivalent metal ions. By selecting suitable ligands and metal ions, ECDs based on CONASHs could exhibit large optical contrast, various colors, excellent cycling stability, persistent optical memory, and broadband electrochromic effect from the visible region to the NIR region. Thus, CONASHs are promising electrochromic materials for next-generation ECDs.

2365709x, 2023, 4, Downloaded from https://adv

onlinelibrary. wiley.com/doi/10.1002/admt.202200917 by University Town Of Shenzhen, Wiley Online Library on [23/11/2025]. See the Terms and Conditions (https://onli

and-conditions) on Wiley Online Library for rules of use; OA articles are governed by the applicable Creative Commons License

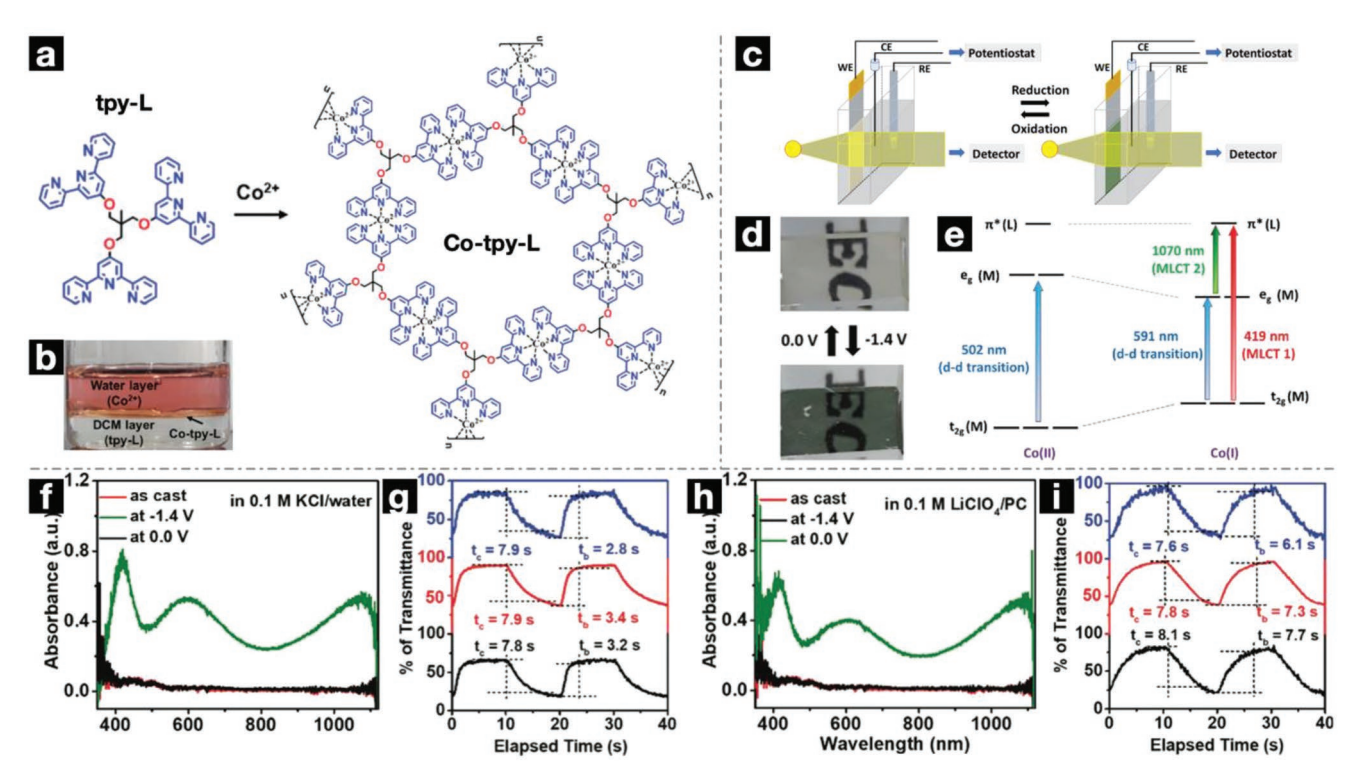


Figure 16. The structures and electrochromic performance of Co-tpy-L CONASHs: a) chemical structures of ligand (4',4""-((2-(((2,2':6',2"-terpyridin)-4'-yloxy)methyl)-2-methylpropane-1,3-diyl)bis(oxy))di-2,2':6',2"-terpyridine) (tpy-L) and synthesized Co-tpy-L nanosheets; b) the synthesized Co-tpy-L film at the liquid–liquid interface; c) schematic diagram of the three-electrode system used for investigating electrochromic properties; d) photographs of the Co-tpy-L film at 0.0 and –1.4 V; e) schematic diagram of possible transitions induced by electrochemical reactions; absorbance curves at different potentials in f) aqueous and h) non-aqueous electrolyte solutions; transmittance versus time in the first two cycles in g) aqueous and i) non-aqueous solutions, respectively; the blue, red, and black lines are for transmittance at 1070, 591, and 419 nm, respectively, in aqueous solution and 1090, 604, and 414 nm, respectively, in non-aqueous solution. Adapted with permission. [46] Copyright 2021, Royal Society of Chemistry.

#### 3.3. MXenes

Transition metal carbides/nitrides/carbonitrides (MXenes), first reported in 2011, are among the latest groups of novel 2D materials and attract a great deal of attention due to their unique hydrophilicity and metallic electrical conductivity. [49] Thus, some people consider MXenes as 2D hydrophilic metals, however, the Fermi levels of MXenes can be modulated by external stimuli, similar to semiconductors, resulting in a wide range of applications, such as nanofiltration, sensors/biosensors, electrocatalyst/photocatalyst, N2 capture and NH3 production, and electronics.<sup>[50]</sup> Typically, MXenes are produced by selectively etching of 'A' elements from the parent MAX phases, which are the precursors of MXenes. The hydrofluoric acid is the most frequently used etchant in this process, and the MXene colloid was then washed and collected for spray coating (Figure 17a).[47] The general formula of MXenes is  $M_{n+1}X_nT_x$  (n = 1-4) with corresponding structures shown in Figure 17b. Elements with a colored background in the periodic table (Figure 17c) can be used to build MXenes, that M is early transition metal, X stands for carbon and/or nitrogen, and  $T_x$  is surface terminations of the outmost transition metal layers (e.g., hydroxyl, oxygen, or fluorine).

The electrochromic effect in MXenes was first reported in 2019 by Gogotsi et al.  $^{[17]}$   $Ti_3C_2T_x$  MXene thin films were synthesized by dip-coating on a glass substrate with an average

thickness of about 30 nm and investigated by in situ UV-vis-NIR spectroscopy under a three-electrode system (Figure 18a). Two thin films functioned as the working and the counter electrode, respectively, and the reference electrode was a silver wire, with the electrolyte of 1 mol L<sup>-1</sup> phosphoric acid (H<sub>3</sub>PO<sub>4</sub>) polyvinyl alcohol (PVA) gel. There was a broad Faradaic contribution and a capacitive envelope in the potential range from -0.2 to -1.0 V/Ag and from -0.3 to 0.0 V/Ag, respectively, with the open circuit voltage (OCV) of -0.2 V/Ag (Figure 18b). Under cathodic potential (−0.4 to −1.0 V/Ag), the free electron density of the MXene was increased, which was further amplified by the pseudocapacitive reduction reactions of the  $T_x$  (Ti-O to Ti-OH). Thus, the transversal surface plasmon effect-induced absorption peak at 770 nm was shifted to 660 nm (Figure 18c), with an optical contrast ( $\Delta T$ ) of about 12% at 770 nm in an acidic electrolyte, more significant than 3% in the neutral electrolyte. Under anodic potential (-0.2 to 0.1 V/Ag), the absorption peak was shifted to 780 nm at 0.1 V/Ag with a slight decrease in transmittance (Figure 18d). Higher voltages than 0.1 V/Ag would lead to an irreversible increase in transmittance and oxidation of  $Ti_3C_2T_x$ . The 90% response time was 0.64 s, with transmittance changing of about 20% (Figure 18e). A reversible color change between green and blue could be obtained in the voltage of 0.0 and -1.0 V/Ag, respectively. This research opens avenues for MXenes in the field of electrochromism.

2365709x, 2023, 4, Downloadec

.com/doi/10.1002/admt.202200917 by University Town Of Shenzhen, Wiley Online Library on [23/11/2025]. See the Terms

ons) on Wiley Online Library for rules of use; OA articles are governed by the applicable Creative Commons License

www.advancedsciencenews.com www.advmattechnol.de

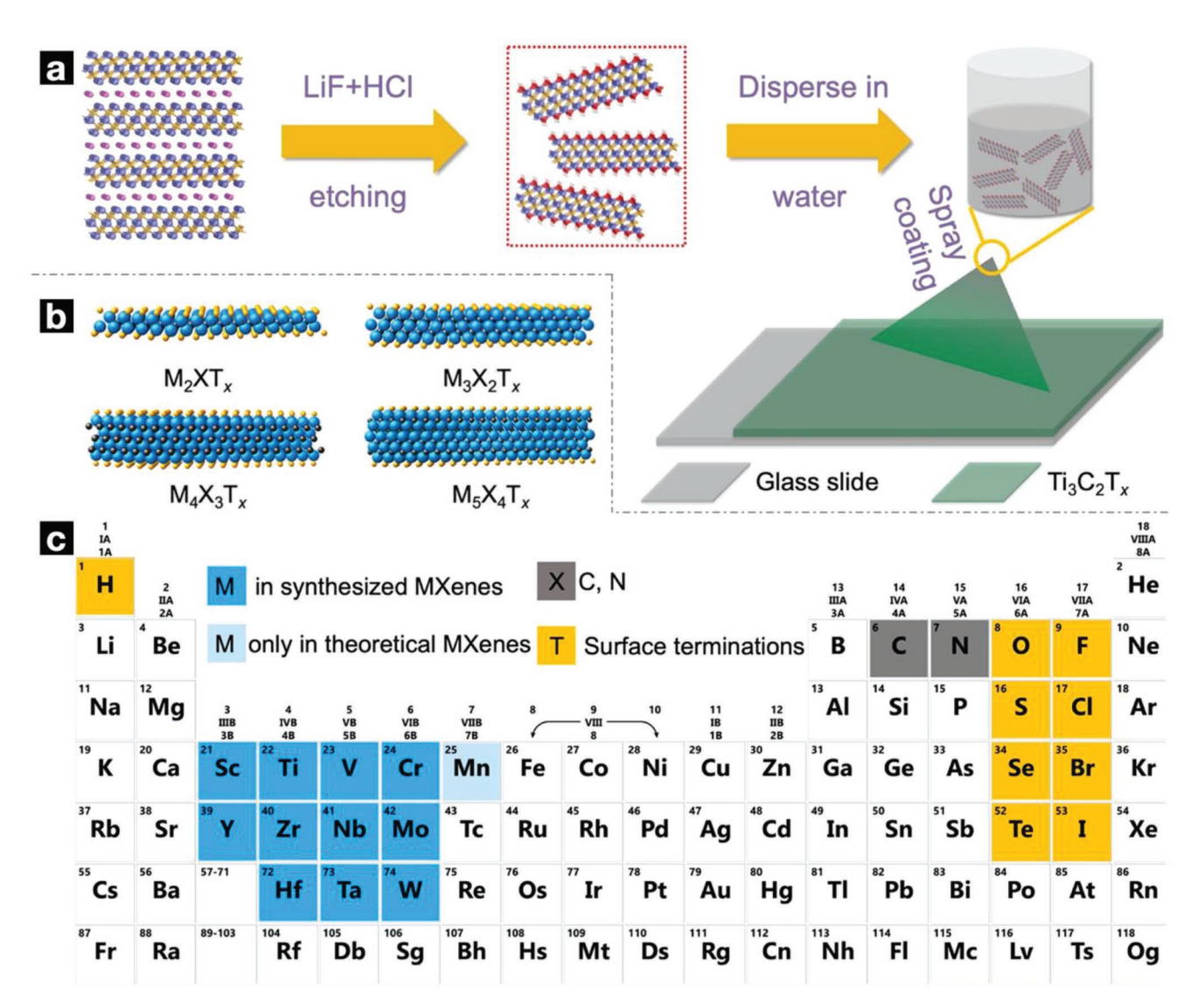


Figure 17. The synthesis and compositions of MXenes: a) schematic illustration of a MXene thin film synthesized via spray coating, where Ti, Al, C, O, and H atoms are shown in blue, purple, yellow, red, and white, respectively; b,c) four typical MXene structures (b), with colors standing for elements in the periodic table (c). a) Adapted with permission.<sup>[47]</sup> Copyright 2021, John Wiley and Sons. b,c) Adapted with permission.<sup>[48]</sup> Copyright 2021, American Chemical Society.

Gogotsi et al.<sup>[51]</sup> further investigated the relationship between the plasmonic behavior and electrochromic properties by employing four different titanium-based MXene thin films via a three-electrode system for in situ opto-electrochemical characterization (19a). The plasmonic extinction peaks under OCV for Ti<sub>3</sub>C<sub>2</sub>T<sub>x</sub>, Ti<sub>2</sub>CT<sub>x</sub>, and Ti<sub>1.6</sub>Nb<sub>0.4</sub>CT<sub>x</sub> were approximately at 800, 550, and 480 nm, respectively (Figure 19b). By decreasing the cathodic potential to -1 V (vs Ag wire) with respect to OCV, these peaks were shifted to 630, 470, and 410 nm, respectively. While for Ti<sub>3</sub>CNT<sub>x</sub>, there was a broad reversible transmittance change of 6.3-10% at 600-400 nm, and the inflexion point of extinction at 670 nm (OCV) gradually disappeared. The maximum changes in the transmittance curves were at 500, 480, 380, and 350 nm for Ti<sub>3</sub>C<sub>2</sub>T<sub>x</sub>, Ti<sub>3</sub>CNT<sub>x</sub>, Ti<sub>2</sub>CT<sub>x</sub>, and Ti<sub>16</sub>Nb<sub>04</sub>CT<sub>x</sub>, respectively. As shown in Figure 19c, Ti<sub>3</sub>C<sub>2</sub>T<sub>x</sub> could achieve the transmittance change of up to 8% for over 2000 cycles, and the value for  ${\rm Ti_3CNT_x}$  was 6.8%, which dropped to 4.3% after 1000 cycles. Irreversible transmittance changes could be observed in  ${\rm Ti_2CT_x}$  and  ${\rm Ti_{1.6}Nb_{0.4}CT_x}$ . The 90% response times were in the range of 0.7–14 s (Figure 19d), dependent on the intrinsic electronic conductivity as no external conducting electrodes were used. Thus, MXene-based ECDs can be modulated in the entire visible spectrum and show potential in optoelectronic, plasmonic, and photonic applications.

Besides acidic aqueous electrolytes, Gogotsi et al. [47] also used three different salts, namely lithium bis(trifluoromethyl sulfonyl)imide (TFSI), 1-ethyl-3-methyl-imidazolium (EMIM) TFSI, and LiClO<sub>4</sub>, in PC solvent to investigate the electrochromic behavior of  $\mathrm{Ti_3C_2T_x}$  in organic electrolyte. The fabricated  $\mathrm{Ti_3C_2T_x}$  flakes via etching processes were 200–300 nm in lateral dimension with a thickness of about 50 nm, followed by spray coating to prepare  $\mathrm{Ti_3C_2T_x}$  films. A typical three-electrode

2365709x, 2023, 4, Downloaded from https://adv

ced.onlinelibrary.wiley.com/doi/10.1002/admt.202200917 by University Town Of Shenzhen, Wiley Online Library on [23/11/2025]. See the Terms and Condition

und-conditions) on Wiley Online Library for rules of use; OA articles are governed by the applicable Creative Commons License

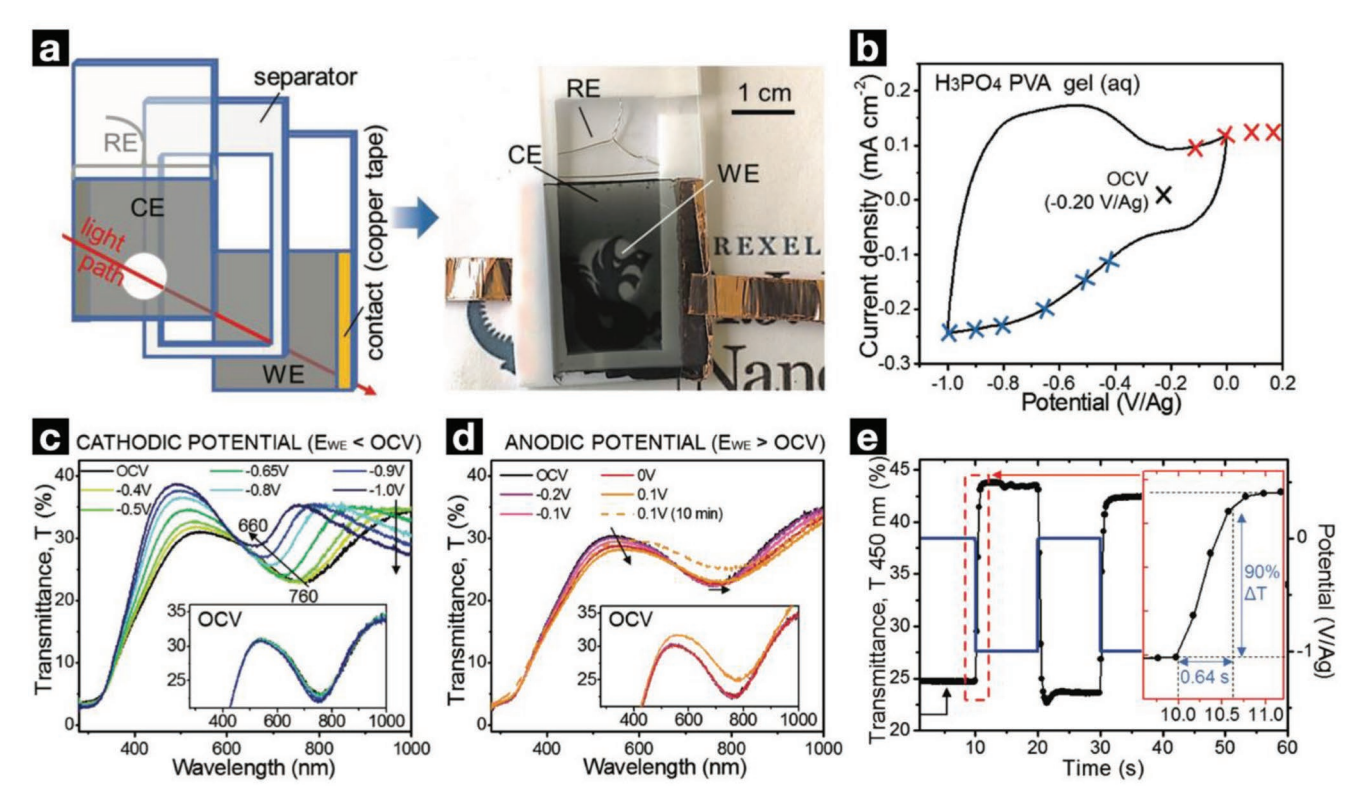


Figure 18. The electrochromic performance of  $Ti_3C_2T_x$  MXene thin films: a) schematic of the three-electrode system used for investigating electrochromic properties and corresponding digital photograph of the device; b) the CV profile of the  $Ti_3C_2T_x$  film, with red and blue cross marks indicating anodic and cathodic potentials, respectively; transmittance spectra under different c) cathodic and d) anodic potentials, respectively, with insets displaying the %T reversibility to OCV; e) transmittance versus time at 450 nm (black) under cyclic potential (blue). Adapted with permission. Copyright 2019, John Wiley and Sons.

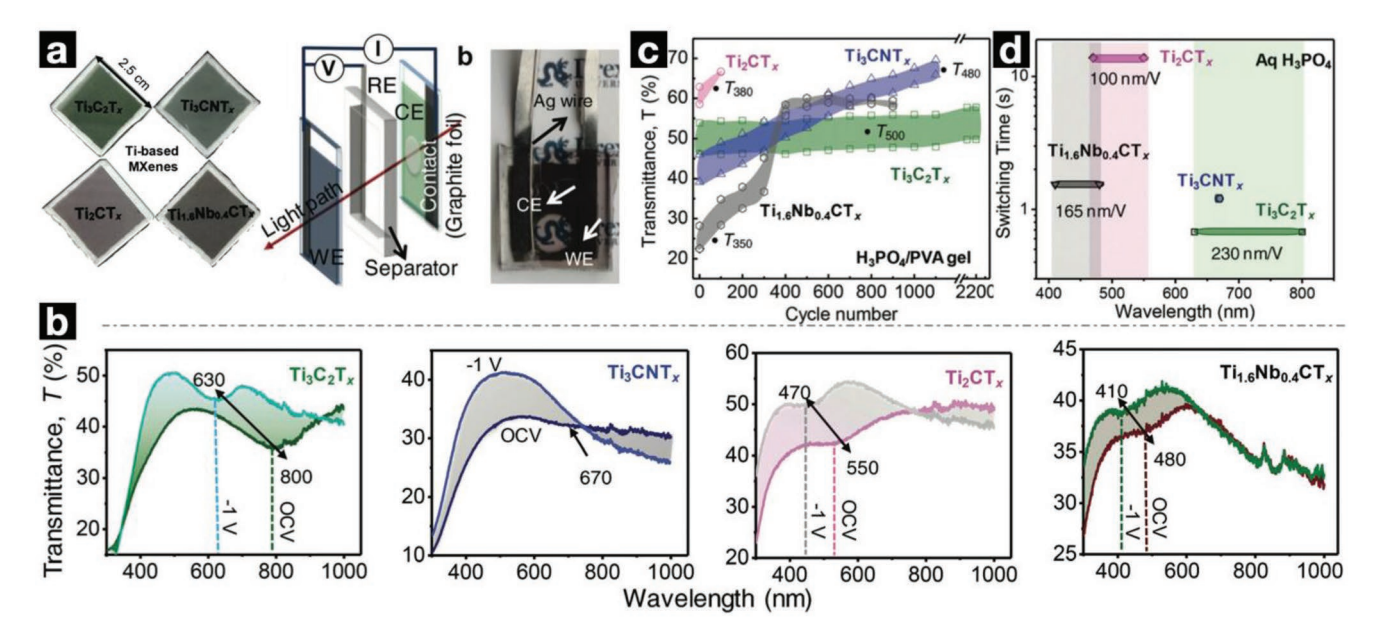


Figure 19. The electrochromic performance of four different titanium-based MXene thin films: a) left: the digital photograph of four titanium-based MXene thin films ( $Ti_3C_2T_x$ ,  $Ti_3CNT_x$ ,  $Ti_2CT_x$ , and  $Ti_{1.6}Nb_{0.4}CT_x$ ); right: in situ opto–electrochemical characterization device; b) transmittance spectra under OCV and cathodic potentials; c) changes of transmittance at 500, 480, 380, and 350 nm for  $Ti_3C_2T_x$ ,  $Ti_3CNT_x$ ,  $Ti_2CT_x$ , and  $Ti_{1.6}Nb_{0.4}CT_x$ , respectively; d) switching time (90% ΔT) with the wavelength shift. Adapted with permission.<sup>[51]</sup> Copyright 2020, Royal Society of Chemistry.

2365709x, 2023, 4, Downl

onlinelibrary. wiley. com/doi/10.1002/admt.202200917 by University Town Of Shenzhen, Wiley Online Library on [23/11/2025]. See the Terms and Conditions (https:

of use; OA articles are governed by the applicable Creative Commons

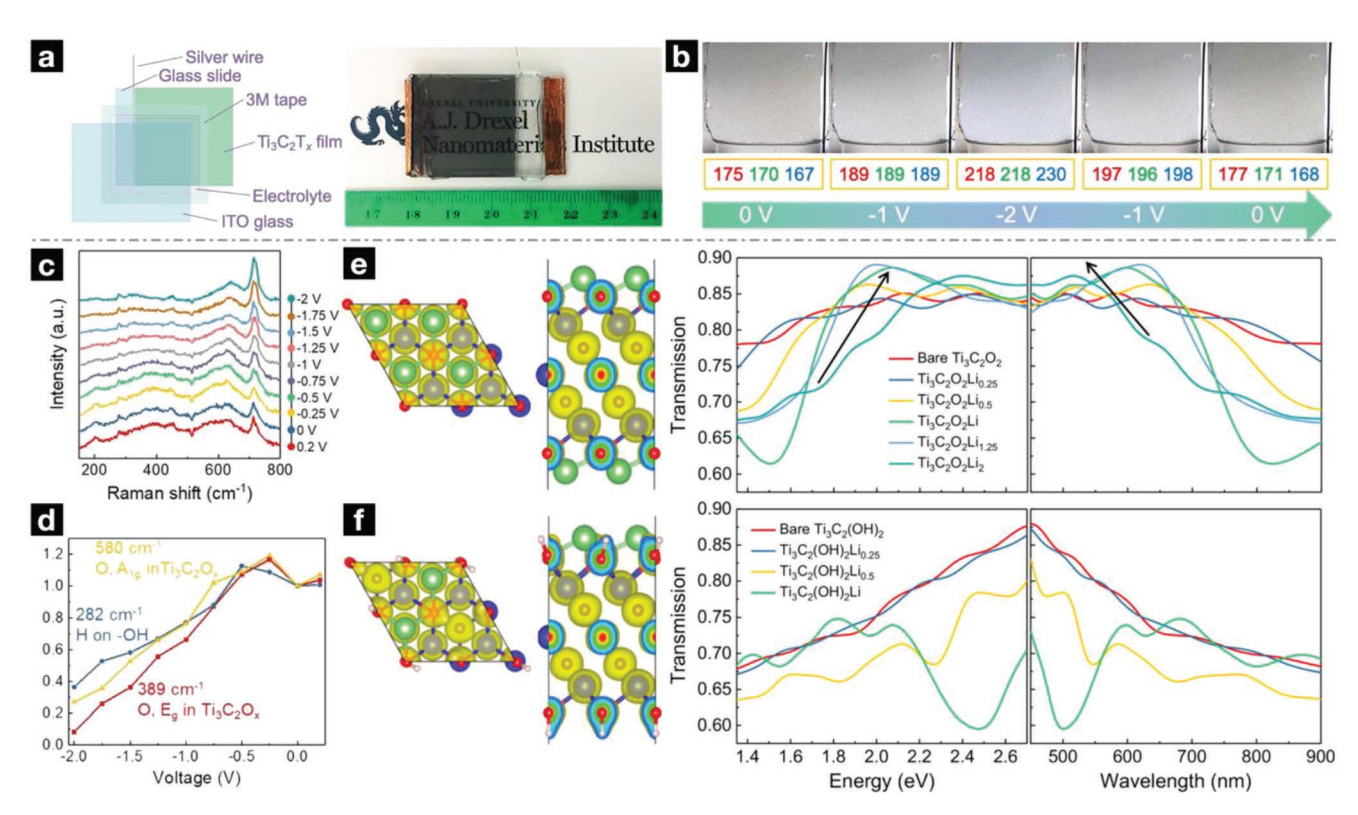


Figure 20. The electrochromic performance of  $Ti_3C_2T_x$  flakes: a) schematic of the fabricated three-electrode cell used for investigating in situ electrochromic properties and corresponding photograph; b) digital images of the device under potentials in the range of 0 to -2 V with corresponding redgreen–blue (RGB) values; c) Raman spectra and d) corresponding statistical results of the peak intensities at 282, 389, and 580 cm $^{-1}$ , corresponding to H atoms (- OH) and O atoms ( $E_g$  and  $A_{1g}$  vibrational modes), respectively; calculated charge density and optical transmission of e)  $Ti_3C_2O_2Li_x$  and f)  $Ti_3C_2(OH)_2Li_x$  on energy and wavelength scales, with black arrows indicating the main peak shift during lithiation. Adapted with permission. Copyright 2021, John Wiley and Sons.

system was used for in situ electrochemical and electrochromic tests, with Ti<sub>3</sub>C<sub>2</sub>T<sub>x</sub>-coated glass as the working electrode, ITO glass as the counter electrode, and a silver wire as the reference electrode (Figure 20a). By reducing the applied voltage from 0 to -2 V in 1 mol L<sup>-1</sup> LiTFSI/PC solution, transparent  $Ti_3C_2T_x$ reversibly changed the color from green (0 V) to blue (-2 V) in Figure 20b. The d-spacing of Ti<sub>3</sub>C<sub>2</sub>T<sub>r</sub> flakes was increased from 12.74 to 15.25 Å after pre-cycling in these three electrolytes, larger than the size of Li<sup>+</sup> or EMIM<sup>+</sup> ions. Thus, the interlayer space of Ti<sub>3</sub>C<sub>2</sub>T<sub>x</sub> flakes was almost kept constant during cycling in the three electrolytes. From the in situ Raman spectra and corresponding statistics in Figure 20c,d, more considerable changes in the vibrational modes of O atoms than that of H atoms in the hydroxy groups indicated stronger interaction between Li ions and the O-terminated MXene surface than with hydroxy groups terminations. DFT calculations found that after lithium intercalation, the formed O-Li bonds introduced a new excitation path at ≈2 eV, resulting in the optical transmittance peak of 500-650 nm (1.9-2.5 eV), as shown in Figure 20e,f. By associating changes in the band structure and charge transfer with the electrochromic shifts, theoretical results confirmed that the O-terminated surfaces and the intercalated species dominated the electrochromic behavior. This study provides further insights into the electrochromic mechanism of Ti<sub>3</sub>C<sub>2</sub>T<sub>x</sub> and lays the foundation for designating high-performance electrochromic MXenes in the future.

Another four electrolytes, namely LiClO<sub>4</sub>, LiBF<sub>4</sub>, NaClO<sub>4</sub>, and tetrabutylammonium tetrafluoroborate (TBABF<sub>4</sub>), were investigated by Rosen et al.<sup>[52]</sup> for non-titanium-based MXenes, Nb<sub>1.33</sub>C nanosheets. The Nb<sub>1,33</sub>C MXene was prepared by etching the solid solution (Nb2/3Sc1/3)2AlC MAX phase to remove the Sc and Al atoms (Figure 21a,b). The Nb<sub>1,33</sub>C film spin-coated on ITO glass (Figure 21c) was studied by in situ UV-vis-NIR spectroscopy. In the electrolyte of 1 mol L<sup>-1</sup> LiClO<sub>4</sub>/PC, Nb<sub>1,33</sub>C MXene switched to the colored state at 1.3 V and the bleached state at 5.3 V, resulting in the optical contrast of 75% at 700 nm (Figure 21d). Similar transmittance curves were observed in LiBF<sub>4</sub> and NaClO<sub>4</sub> electrolytes (Figure 21e). However, no significant transmittance difference of Nb<sub>1.33</sub>C was shown in the electrolyte of TBABF<sub>4</sub> ( $\Delta T\%$  < 10%) due to the irreversible ion migration. An ECD of Nb<sub>1,33</sub>C was fabricated with the structure of ITO/ Nb<sub>1,33</sub>C/electrolyte/ITO (Figure 21f). The contrast ratio could be up to 80% at 700 nm (Figure 21g) and about 77% at 1200 nm (Figure 21h), with excellent optical memory effect and cycling stability originating from the loosely arranged structure of Nb<sub>1,33</sub>C and negligible traps in the intercalation process. This research dramatically improves the electrochromic performance of MXenes and is a big step forward for practical applications in modulating transmittance from visible to NIR regions.

Although research in electrochromic MXenes is still in its initial stage with only four related papers, the diversity of composition and structures as well as unique physical and

2365709x, 2023, 4, Downloaded from https://adv

ced online library. wiley.com/doi/10.1002/admt.202200917 by University Town Of Shenzhen, Wiley Online Library on [23/11/2025]. See the Terms and Conditions (https://onlinelibrary.wiley.c

and-conditions) on Wiley Online Library for rules of use; OA articles are governed by the applicable Creative Commons License

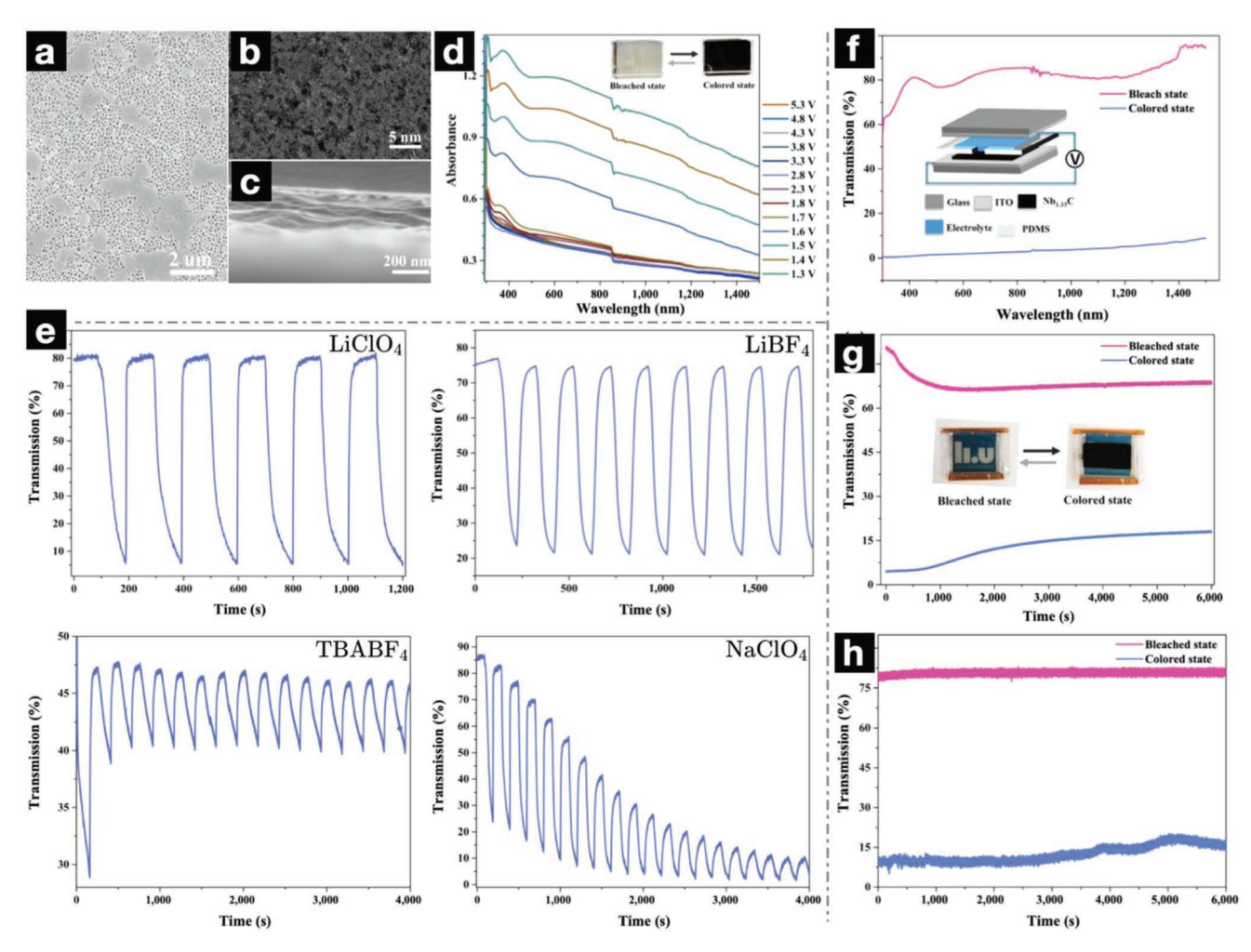


Figure 21. The morphology and electrochromic performance of Nb<sub>1,33</sub>C nanosheets: a) a SEM image of Nb<sub>1,33</sub>C nanosheets; b) a high-magnification STEM image of Nb<sub>133</sub>C single flake; c) a cross-sectional image of the Nb<sub>133</sub>C film (middle) deposited on the ITO glass (top); d) the absorption spectra of the Nb<sub>133</sub>C film under various potentials, with the inset showing the photographs at bleached and colored states; e) transmission at 700 nm under the cyclic voltage between 1.3 and 5.3 V (vs Li/Li<sup>+</sup>) in four different electrolytes; f) the wavelength dependence of transmission of the fabricated ECD, with the inset showing the device structure; transmission versus time of the ECD at g) 700 nm and h) 1200 nm, with the inset showing the device at bleached and colored states. Adapted with permission.<sup>[52]</sup> Copyright 2022, Springer Nature.

chemical properties of MXenes brings in tremendous potential for next-generation ECDs with better electrochemical and electrochromic properties as well as multifunctionality. Moreover, MXenes have ultrahigh electronic conductivity and can work as both electrochromic materials and conducting layers to simplify structures and reduce the costs of ECDs.

### 3.4. Others

Adv. Mater. Technol. 2023, 8, 2200917

In addition to the aforementioned materials, some other 2D materials with the electrochromic effect have also been reported. As early as 1965, Hennig discovered that the lamellar compounds ( $C_8Cs$ ,  $C_9AlCl_{3.3}$ , dilute  $C_nCs$ , and  $C_{11}FeCl_3$ ) had increased transmittance than graphite over a wide range of wavelengths. However, the conductivity of the compounds in the direction of c axis was an order of magnitude higher than that of graphite, suggesting the absorption mechanism

of plasma oscillations. In 2014, Hu et al.[12] simultaneously measured in situ optical transmittance and electrical conductivity of ultrathin graphite materials of 3-60 graphene layers in thickness via a sandwich-structured cell with electrolyte of 1 mol  $L^{-1}$  LiPF<sub>6</sub> in w/w = 1/1 ethylene carbonate (EC)/diethyl carbonate (DEC). As shown in Figure 22a-d, significant increasements could be observed in the optical transmittance (74.4-90.98% and 55.9-79.2% for 18- and 38-layer graphite, respectively) and electrical conductivity (approximately two orders of magnitude). This apparent contradiction came from the unique band structure of the graphene layer where lithium intercalation shifted the Fermi level upward and inhibited interband transitions due to the Pauli exclusion principle, resulting in higher transmittance in the visible region. Meanwhile, intercalation increased the carrier concentration, which led to better conductivity. Similar changes in transmittance are presented in Figure 22e using encapsulated commercially obtained CVDgrown thin graphite.

2365709x, 2023, 4, Downloaded

nlinelibrary.wiley.com/doi/10.1002/admt.202200917 by University Town Of Shenzhen, Wiley Online Library on [23/11/2025]. See the Terms

iditions) on Wiley Online Library for rules of use; OA articles are governed by the applicable Creative Commons License

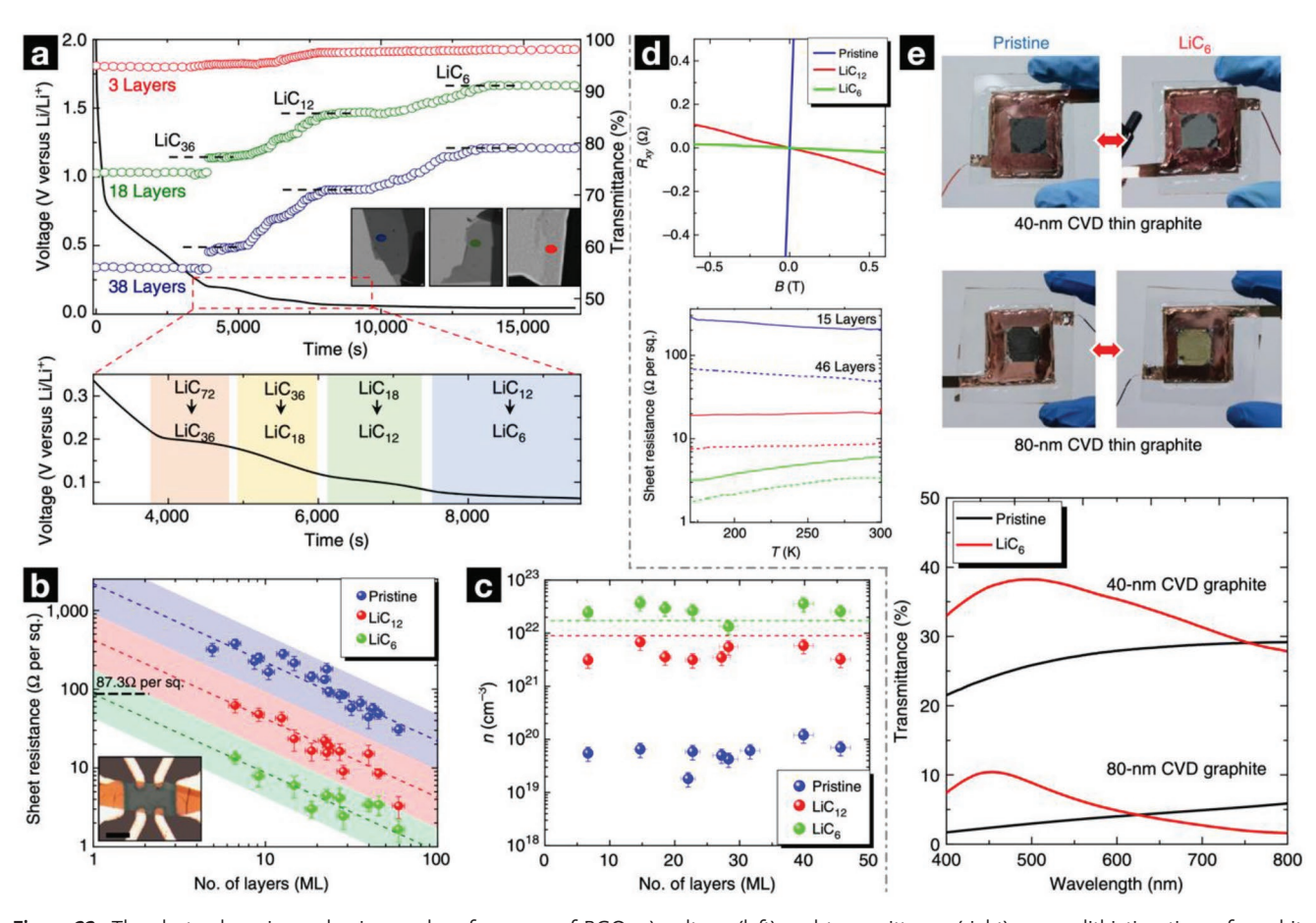


Figure 22. The electrochromic mechanism and performance of RGO: a) voltage (left) and transmittance (right) versus lithiation time of graphite materials with different layers, with four intercalation stages shown in the enlarged image below; b) resistivity and c) carrier density as a function of graphite thickness; d) Relationship between Hall resistance and magnetic field as well as temperature-dependent sheet resistance; e) demonstration of transparent electrodes using commercially obtained 40- and 80-nm CVD-grown thin graphite and corresponding transmittance spectra before and after lithium intercalation. Adapted with permission.<sup>[12]</sup> Copyright 2014, Springer Nature.

After the pioneering work of limited transmittance modulation in graphite materials, Hu et al. [53] improved the electrochromic performance via sodium-ion intercalation of RGO, which was inhibited in pristine graphene due to the limited interlayer distance (3.35 Å). Before and after Na-ion intercalation, the interlayer distances of RGO film were 3.49 and 3.76 Å, respectively, obtained via XRD. The reversible specific capacity was 0.028 Na per carbon atom, calculated from the reversible capacity in Figure 23a. A lateral RGO network device was fabricated (Figure 23b), which helped capture the optical microscope images during sodiation (Figure 23c). A typical increase of transmittance after sodiation was from 36% to 79% (Figure 23d), with wavelength-dependent spectra shown in Figure 23e. Meanwhile, the device based on the Na-RGO network had much better air stability than Li-intercalated graphene, with only a slight decrease in transmittance after 13 h (Figure 23f). This was mainly due to the self-terminating oxidation processes between Na ions and water, carbon dioxide, or oxygen at the RGO edges. Similar to the graphite materials, transmittance increased with electrical conductivity due to the same mechanism.

Besides graphite materials, copper chalcogenides have also been reported for the electrochromic effect. Chinnapiyan

et al.[15] synthesized CuSe thin film on ITO glass via electrodeposition, with grain sizes between 53.33 and 93.33 nm. The energy gap was 1.78 eV, and two absorption peaks were observed at 300 and 900 nm. The former band at 300 nm came from the  $\pi$ – $\pi$ \* transitions, while the latter 900 nm band could be attributed to the formation of subgap states. The absorbance increased with the applied voltage from -0.8 to 0.8 V, with the color changing from yellowish red to contrasting yellow. The optical contrast ( $\Delta T$ ) was 81% at 300 nm with the CE of 620 cm<sup>2</sup> C<sup>-1</sup>. The response times for coloring and bleaching were 18 and 21 s, respectively. Although, CuSe was similar to CuS in compositions, chemical bonds, and crystal structures. However, the electrochromic mechanisms for CuSe and CuS are different. The former is mainly based on interband absorption, while it is the localized surface plasmon resonance (LSPR) properties for the latter. Tatsuma et al.[14] synthesized CuS nanoplates which could tune the NIR localized plasmon via redox reactions. Corresponding schematic diagram and CV curves are shown in Figures 24a and 24b, respectively. The absorbance modulation range at about 1300 nm was around 0.27 (Figure 24c,d), due to the disappearance and recovery of LSPR, with negligible changes in the visible region. During

2365709x, 2023, 4, Downloaded from https://adv

onlinelibrary.wiley.com/doi/10.1002/admt.202200917 by University Town Of Shenzhen, Wiley Online Library on [23/11/2025]. See the Terms

and-conditions) on Wiley Online Library for rules of use; OA articles are governed by the applicable Creative Commons License

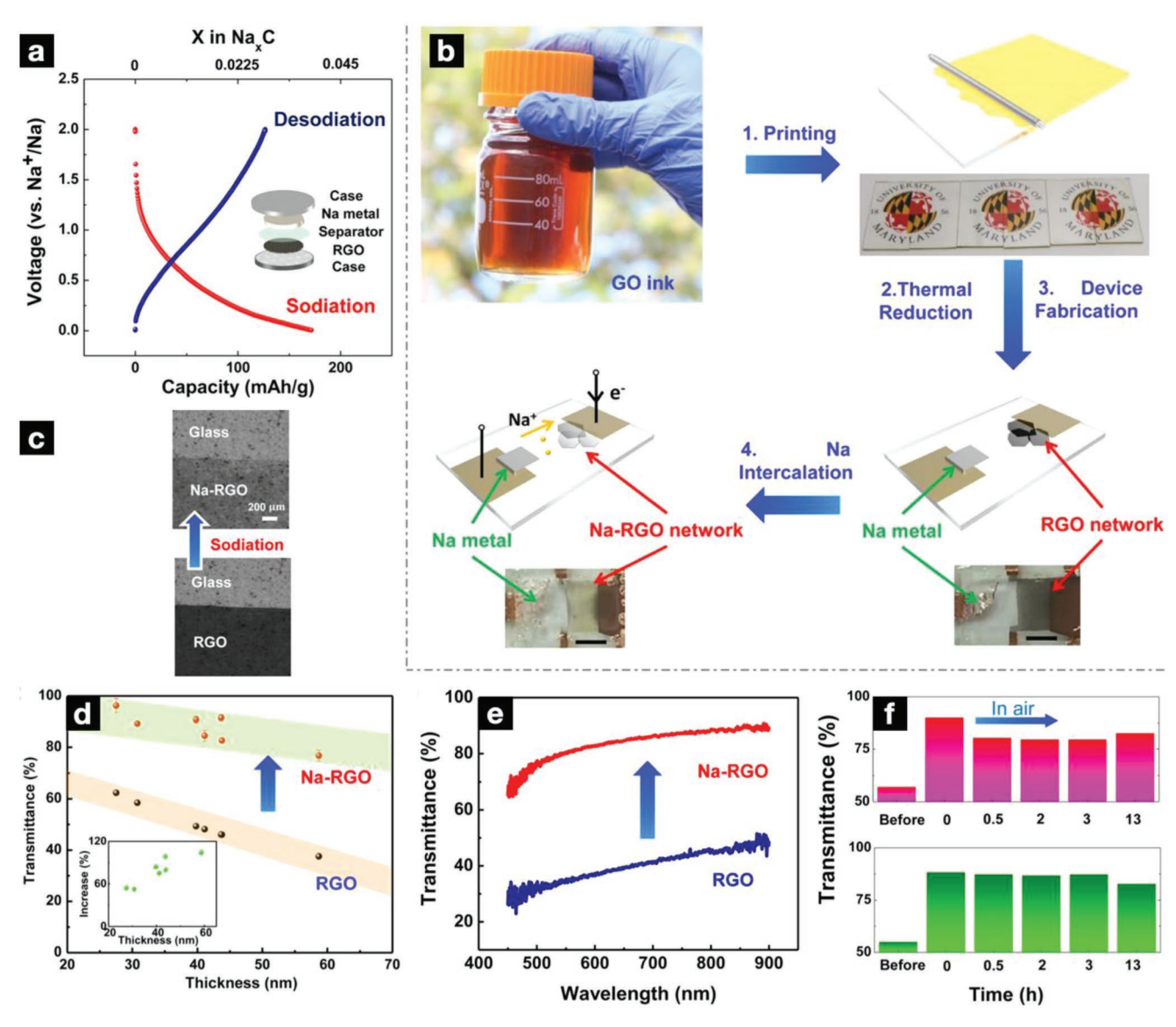


Figure 23. The electrochromic performance of RGO via Na intercalation: a) voltage profile (second cycle) of sodium intercalation/deintercalation in RGO network; b) demonstration of high-performance transparent electrodes based on Na-ion intercalated RGO; c) grayscale images by an optical microscope before and after Na-ion intercalation; d) transmittance as a function of RGO network thickness before and after sodiation at 550 nm, with the inset of corresponding relative increase; e) the wavelength dependence of transmittance in the range of 450–900 nm; f) transmittance versus time of transparent conductor based on Na-RGO network for evaluating the air stability. Adapted with permission.<sup>[53]</sup> Copyright 2015, American Chemical Society.

voltage switching in the range of -0.6 to -1.0 V, the transmittance changed between  $\approx 30\%$  and  $\approx 80\%$  reversibly (Figure 24e). The coloration (oxidation) and bleaching (reduction) times were 5.3 and 2.3 s, respectively, with a CE of 30–40 cm<sup>2</sup> C<sup>-1</sup>. The fast responses could be explained by the thin nanoplate structure with a high specific area and the surface redox reactions. These two studies indicate that the transition metal chalcogenides might be a group of promising electrochromic materials for optical and thermal modulation.

Cao et al.<sup>[18]</sup> synthesized a highly porous HOF film via self-assembly of 1,3,6,8-tetrakis(*p*-benzoic acid) pyrene (H<sub>4</sub>TBAPy), denoted as nano-PFC-1, which was deposited on FTO glass in CH<sub>2</sub>Cl<sub>2</sub> solution through electrophoretic depo-

sition (EPD) method with an average thickness of 500 nm (**Figure 25a**). There were two peaks in the CV curves, an anodic peak at 1.23 V and a cathodic peak at 1.19 V, resulting in the color change from yellow to blue–violet (Figure 25b). The electrochemical processes were capacitance-dominant, indicating a fast charge transfer rate, as the fitted value of b for the anodic and cathodic peaks in the equation ( $i = av^b$ ) was 0.76 and 0.87, respectively. The long-term CV scans of amorphous H<sub>4</sub>TBAPy film and nano-PFC-1 are shown in Figure 25c, respectively. Due to the high crystallinity and structural stability of  $\pi$  stacking, only a slight decrease could be observed in nano-PFC-1 after 500 cycles, in sharp contrast with the amorphous H<sub>4</sub>TBAPy. Moreover, the HOF materials

2365709x, 2023, 4, Downloaded from https://advanced.onlinelibrary.wiley.com/doi/10.1002/admt.202200917 by University Town Of Shenzhen, Wiley Online Library on [23/11/2025]. See the Terms and Conditions (https://doi.org/10.1002/admt.20200917 by University Town Of Shenzhen, Wiley Online Library on [23/11/2025]. See the Terms and Conditions (https://doi.org/10.1002/admt.20200917 by University Town Of Shenzhen, Wiley Online Library on [23/11/2025]. See the Terms and Conditions (https://doi.org/10.1002/admt.20200917 by University Town Of Shenzhen, Wiley Online Library on [23/11/2025]. See the Terms and Conditions (https://doi.org/10.1002/admt.20200917 by University Town Of Shenzhen, Wiley Online Library on [23/11/2025]. See the Terms and Conditions (https://doi.org/10.1002/admt.20200917 by University Town Of Shenzhen, Wiley Online Library on [23/11/2025].

and-conditions) on Wiley Online Library for rules of use; OA articles are governed by the applicable Creative Commons License

**4DVANCED** 

Figure 24. a) Schematic diagram of NIR tuning of CuS nanoplates; b) current and c) absorbance curves of CuS nanoplates on the ITO glass during voltage scanning in the range of -0.63 to -1.0 V (vs Ag/AgCl); d) absorbance spectra of CuS nanoplates deposited on the ITO glass under different potentials, with the inset showing the photos of the electrode at -0.6 and -1.0 V; e) transmittance changes of the CuS nanoplates on the ITO glass under cyclic potentials between -0.6 and -1.0 V. Adapted with permission. [14] Copyright 2016, Royal Society of Chemistry.

Potential / V vs. Ag I AgCI

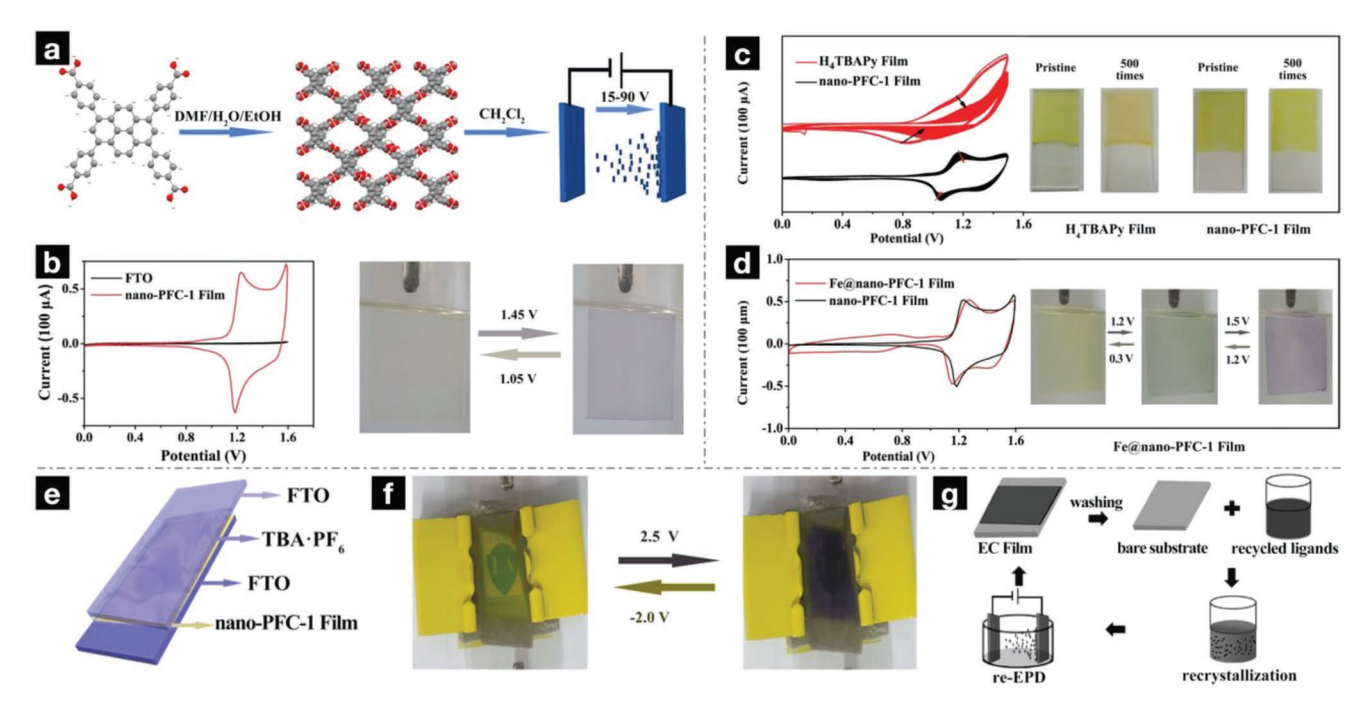


Figure 25. The synthesis and electrochromic performance of nano-PFC-1 film: a) the preparation method for the nano-PFC-1 film via EPD (C: gray, H: white, O: red); b) CV curves of the pristine nano-PFC-1 film and FTO glass at a scan rate of 5 mV s<sup>-1</sup> and corresponding digital photographs at 1.45 and 1.05 V (vs Ag/AgCl); c) CV scanning for 500 cycles at a scan rate of 20 mV s<sup>-1</sup>, with corresponding digital photographs of the H<sub>4</sub>TBAPy film (left) and nano-PFC-1 film (right) in the pristine state and after 500 cycles; d) CV spectra of the Fe@nano-PFC-1 and nano-PFC-1 films at a scan rate of 5 mV s<sup>-1</sup>, with corresponding images of Fe@nano-PFC-1 film under different potentials; e) schematic structure for the ECD based on PFC-1 film; f) the fabricated ECD switching between transparent (-2.0 V) and opaque (2.5 V) states; g) regeneration procedures for the electrochromic films. Adapted with permission.<sup>[18]</sup> Copyright 2020, John Wiley and Sons.

www.advancedsciencenews.com www.advmattechnol.de

 Table 1. Summary of the electrochromic performance of reported 2D materials.

Electrochromic films [electrolytes]	Color change	Wavelength [nm]	Optical Contrast [ΔT %]	Response time for Coloration/bleaching [s]	oloration Efficiency [cm² C <sup>-1</sup> ]	Stability [cycles or $\Delta T\%$ decay]	Year and Ref.
COF <sub>3PA-TT</sub> /ITO (0.1 mol L <sup>-1</sup> LiClO <sub>4</sub> /PC)	deep red and dark brown	610 1300	16% 15%	18.5/7 (90%) 20/2.5 (90%)	104 56	-1.5% (15 cycles); -0.6% (15 cycles)	2019 [16]
$COF_{TPDA-PDA}/ITO$ (0.1 mol $L^{-1}$ NaClO <sub>4</sub> /CH <sub>3</sub> CN)	plum, gray and light blue	1050	52%	1.3/0.7 (90%)	320	>1000 cycles	2021 [25]
EC-COF-1/ITO (LiClO <sub>4</sub> /PC-based PMMA polymer gel)	blue purple and transparent	574 730	33% 12%	1.8/7.2 (90%) 2.6/3.5 (90%)	284 246	>200 cycles	2020 [26]
Py-ttTII/ITO (0.1 mol L <sup>-1</sup> TBAPF <sub>6</sub> / CH <sub>3</sub> CN)	dark green and black	550	1.2 OD (ΔA %)	0.38/0.2 (10–90%)	318	>200 cycles	2021 [27]
1-Fe/ITO (1 mol L <sup>-1</sup> Bu <sub>4</sub> NClO <sub>4</sub> / CH <sub>3</sub> CN)	deep purple and pale yellow	578 nm	≈67% (∆A %)	0.35	-	>800 cycles	2015 [13]
2-Fe/ITO (1 mol L <sup>-1</sup> Bu <sub>4</sub> NClO <sub>4</sub> / CH <sub>3</sub> CN)	deep violet and pale yellow	590 nm	≈37% (∆A %)	0.54	-	>1000 cycles	
1-Co/ITO (1 mol L $^{-1}$ Bu $_4$ NClO $_4$ -CH $_2$ Cl $_2$ )	orange and deep purple	≈600 nm	≈17% (∆A %)	-	-	-	
NBP1/ITO (0.1 mol L <sup>-1</sup> LiClO <sub>4</sub> / CH <sub>3</sub> CN)	blue and colorless	590 nm	62%	0.48/0.57 (95%)	431	>1500 cycles	2019 [41]
NBP2/ITO (0.1 mol L <sup>-1</sup> LiClO <sub>4</sub> / CH <sub>3</sub> CN)	magenta and yellow	568 nm	57%	0.50/0.54 (95%)	382	>1500 cycles	
Co-S1/ITO (1 mol L <sup>-1</sup> TBAPF <sub>6</sub> /CH <sub>2</sub> Cl <sub>2</sub> )	red and green	500 nm	21% (ΔA %)	_	123.76	180 s (36 cycles)	2019 [42]
Co-S2/ITO (1 mol L <sup>-1</sup> TBAPF <sub>6</sub> /CH <sub>2</sub> Cl <sub>2</sub> )	light red and orange	540 nm	18% (∆A %)	_	91.88	100 s (20 cycles)	
Fe(II)+TPA-TPY/ITO (0.1 mol L <sup>-1</sup> Bu <sub>4</sub> NCIO <sub>4</sub> /CH <sub>3</sub> CN)	purplish red, orange yellow and green	580 nm	22.3%	0.5/0.4 (95%)	141.72	>500 cycles	2019 [43]
Fe(II)+L <sub>3Phn</sub> /ITO (0.1 mol L <sup>-1</sup> LiClO <sub>4</sub> nonaqueous solution)	intense red and colorless	518 nm	55%	2.9/3.3	230	>15 000 cycles	2020 [44]
3tpy-Fe/ITO (0.1 mol L $^{-1}$ LiClO $_4$ / CH $_3$ CN)	intense pink and colorless	556 nm	53%	1.15/2.49 (95%)	470.16	-4.91% (5 s for 500 cycles); -2.91% (10 s for 1000 cycles)	2020 [45]
Co-tpy-L/ITO (0.1 mol L <sup>-1</sup> KCI/water)	colorless and blackish green	419 nm 591 nm 1070 nm	48.3% 54.1% 61.3%	7.8/3.2 (95%) 7.9/3.4 (95%) 7.9/2.8 (95%)	115.8	up to 1500 s	2021 [46]
Co-tpy-L/ITO (0.1 mol L <sup>-1</sup> LiClO <sub>4</sub> /PC)	colorless and blackish green	414 nm 604 nm 1090 nm	57.2% 58.6% 64.6%	8.1/7.7 (95%) 7.8/7.3 (95%) 7.6/6.1 (95%)	211	>7500 s	
$Ti_3C_2T_x/glass$ substrate (1 mol L <sup>-1</sup> $H_3PO_4/PVA$ gel)	green and blue	450 nm 770 nm	20% 12%	0.64 (90%)	-	-	2019 [17]
$Ti_3C_2T_x/g$ lass substrate (1 mol L <sup>-1</sup> $H_3PO_4/PVA$ gel)	pale green to blue	500 nm	8%	0.7 (90%)	-	>2000 cycles	2020 [51]
$Ti_3CNT_x/glass$ substrate (1 mol L <sup>-1</sup> $H_3PO_4/PVA$ gel)	dim gray to trans- parent with violet tint	480 nm	6.8%	1.2 (90%)	-	-4.3% after 1000 cycles	
$Ti_2CT_x/glass$ substrate (1 mol L <sup>-1</sup> $H_3PO_4/PVA$ gel)	pale magenta to transparent with violet tint	550 nm	10%	14 (90%)	-	<100 cycles	
$Ti_{1.6}Nb_{0.4}CT_x/glass$ substrate (1 mol L <sup>-1</sup> $H_3PO_4/PVA$ gel)	tan brown to trans- parent with green tint	480 nm	8.5%	1.5 (90%)	-	$\Delta T \approx 1\%$ for over 350 cycles	
$Ti_3C_2T_x/g$ lass substrate (1 mol L <sup>-1</sup> LiTFSI/PC)	green and blue	428 nm	8%	-	-	>300 cycles	2021 [47]
$Nb_{1.33}C/ITO$ (1 mol $L^{-1}$ LiClO <sub>4</sub> /PC)	colorless, grey, and black	700 nm	75%	68/1.9	96	-4.3% after 1000 cycles	2021 [52]
ultrathin graphite (1 mol $L^{-1}$ LiPF <sub>6</sub> in $w/w = 1/1$ EC/DEC)	opaque and slight transparent	550 nm	23.3%	-	-	-	2013 [12]

Adv. Mater. Technol. 2023, 8, 2200917

www.advancedsciencenews.com

www.advmattechnol.de

Table 1. Continued.

Electrochromic films [electrolytes]	Color change	Wavelength [nm]	Optical Contrast $[\Delta T \%]$	Response time for coloration/bleaching [s]	Coloration Efficiency $[cm^2C^{-1}]$	Stability [cycles or $\Delta T\%$ decay]	Year and Ref.
RGO (1 mol L <sup>-1</sup> NaPF6 in $v/v = 1/1$ EC/DEC)	opaque and transparent	550 nm	45.4%	-	-	-	2015 [53]
CuSe/ITO (0.1 mol L <sup>-1</sup> H <sub>2</sub> SO <sub>4</sub> )	yellowish red and yellow	300 nm	81%	18/21	620	-	2016 [15]
CuS nanoplates/ITO (0.1 mol $L^{-1}$ Na <sub>2</sub> S/deuterated water)	_	1300 nm	50% (ΔT %) 27%(ΔA %)	5.3/2.3	30–40	-	2016 [14]
nano-PFC-1/FTO (0.1 mol $\rm L^{-1}$ TBAPF $_{\rm 6}$ / $\rm CH_2Cl_2$ )	yellow and blue-violet	600 nm	50%	12/14 (90%)	83.7	>500 cycles	2020 [18]
Fe@nano-PFC-1/FTO (0.1 mol L <sup>-1</sup> TBAPF <sub>6</sub> /CH <sub>2</sub> Cl <sub>2</sub> )	yellow, green and blue-violet	_	-	-	-	-	

could be doped with exogenous electroactive species like Fe(II) ions, denoted as Fe@nano-PFC-1. The color reversibly changed from yellow to green and blue-violet when raising the voltage from 0 to 1.2 and 1.5 V, respectively (Figure 25d). In terms of the electrochromic performance, the transmittance modulation range was from 75% (pristine state) to 25% (colored state) during voltage switching between 1.5 and -0.9 V. Corresponding 90% coloration and bleaching times were 12 and 14 s, with the CE value of 83.7 cm<sup>2</sup> C<sup>-1</sup>. A practical ECD was fabricated with the structure of FTO/TBA·PF<sub>6</sub> electrolyte/nano-PFC-1 film/FTO (Figure 25e), and the transmittance change between clear and blurry was shown in Figure 25f. More importantly, the unique structure of HOF allowed for easy recycling and regeneration with procedures established in Figure 25g. The electrochromic HOF materials are promising for ECDs with low energy consumption, durable cycle life, easy renewal, and post-synthetic modification, and these merits are almost impossible for other electrochromic materials.

Although current electrochromic performance of the materials in this section is still limited compared with traditional electrochromic ones, novel materials and structures are constantly emerging with various physical and chemical properties and enrich the scope of 2D electrochromic materials. With continuous efforts from researchers, any challenge will be conquered in this vivifying area.

# 4. Conclusions and Future Challenges

With the rapid development of novel preparation and processing methods, the number of reported emerging 2D electrochromic materials is in rapid growth, and corresponding electrochromic performance has been dramatically improved, summarized in Table 1. In this review, we systematically discussed the latest advances in emerging 2D electrochromic materials, including COFs, CONASHs, MXenes, HOFs, RGO, and copper chalcogenides. Benefiting from their atomically thin thickness, large lateral size, high specific area, abundant exposed active sites, reduced diffusion distances, and multiple pathways for ion transportation, these 2D electrochromic materials exhibit large optical contrast, rapid switching speed,

high CE, and excellent cycling stability, compared with their counterparts in bulk states and traditional electrochromic materials. Meanwhile, 2D electrochromic materials are promising in various applications, especially flexible electronics, due to their intrinsic flexibility derived from 2D structures, which have a vital position in next-generation ECDs.

However, there remains a long way to go before the large-scale commercialization of 2D electrochromic materials and some crucial issues that should be focused on and properly addressed. For COFs, further investigations need to be carried out on the mechanism of the donor–acceptor strategy and its corresponding application range. Armed with design strategies, researchers could synthesize 2D COFs or COF composites with customized functionalities in electronic and optoelectronic devices. Also, the existence of the synthesis method beyond solvothermal polycondensation and cathodic COFs is waiting to be figured out in future research.

Current reported electrochromic CONASHs are synthesized via a bottom-up method at the liquid–liquid interface, which is slow in reaction rate and easily introduces cracks or holes during transferring to substrates. Meanwhile, many CONASHs can be fabricated using the top-down method. However, no electrochromic effect has been reported in these materials. In terms of composition, only ligands based on polypyridyl and metal ions of iron and cobalt are used. The metal–ligand relationship is not clear for future COF design. All these problems appeal for more studies.

For MXenes, due to the diversity of structure and composition, many titanium and non-titanium-based MXenes have not been explored, which could employ theoretical tools for screening before experiments. Further research can focus on the surface chemistry of MXenes, especially the relationship between terminations (other than O atoms and – OH) and electrochromic performance. Defect engineering also can be tried to tune the electrochromic properties. For other emerging 2D electrochromic materials, including HOFs, RGO, and copper chalcogenides, research papers are just starting to emerge, and there is plentiful room for investigation.

Besides these specific problems, there are also some common ones for materials. First, although 2D structures have more voids to relieve the structural distortion induced by intercalation/deintercalation, the long-term cycling stability is

ADVANCED SCIENCE NEWS

www.advancedsciencenews.com

ADVANCED MATERIALS TECHNOLOGIES

www.advmattechnol.de

still a challenge for all materials. Second, environmental conditions, especially temperature and light, have apparent impacts on electrochromic performance. The thermal and light stabilities of 2D electrochromic materials should be considered as well, which are neglected in current research. Third, one of the unique characteristics of 2D materials is their intrinsic flexibility with crystallinity, which could endure large deformability in and out of the plane while maintaining structural integrity. This advantage could be utilized to improve electrochromic performance and design heterostructures in 3D space with desired physical and chemical properties for multifunctional devices.

In addition to the 2D electrochromic materials themselves, current experimental methods also should be improved where most studies use the typical three-electrode system to in situ investigate the electrochromic performance. One ITO glass with deposited electrochromic materials is used as the working electrode and a blank ITO glass as the counter electrode. Compared with the performance of practical ECDs, the measured properties are generally underestimated for two reasons. One is that practical devices usually use cathodic and anodic electrochromic materials deposited on corresponding electrodes, remarkably improving the electrochromic performance. The other is that the counter electrode of ITO glass has a relatively small charge capacity that fails to balance all the charge located on the electrochromic layer, which limits the potential of electrochromic materials in terms of optical contrast and cycling stability. A transparent electrode with large charge-storage capability should be used instead for precise measurements. For practical applications, the charge-storage capacity should be controlled to the same value for the cathodic and anodic electrodes.

Apart from experiments, a large number of theoretical papers have witnessed the success of computational tools, especially DFT and artificial intelligence (AI) like machine learning, in a wide range of areas, that is, energy storage and transformation, catalysis, drug discovery, and even bioscience. With more proposed accurate calculation methods and increasing computing power, computational tools are indispensable in scientific research and should be utilized in 2D electrochromic materials. For example, computational tools can help discover 2D electrochromic materials via high-throughput screening, understand the structure–property relationship, and rationally design 2D materials with customized structures and functionalities. A great deal of time, manpower, and money can be saved, facilitating the rapid development of 2D electrochromic materials.

In the end, the bright future of electrochromic applications requires researchers to keep exploring novel materials, simplifying the synthesis methods, reducing cost, and improving electrochromic performance. Significant progress on 2D electrochromic materials has been achieved, which gives confidence to researchers and incentives them to forge ahead and overcome all challenges encountered.

## **Acknowledgements**

Open access publishing facilitated by Griffith University, as part of the Wiley - Griffith University agreement via the Council of Australian University Librarians.

## **Conflict of Interest**

The authors declare no conflict of interest.

## **Keywords**

electrochromic devices, electrochromism, two-dimensional materials

Received: June 6, 2022 Revised: August 9, 2022 Published online: October 25, 2022

- [1] N. Kobosew, N. I. Nekrassow, Z. Elektrochem. Angew. Phys. Chem. 1930, 36, 529.
- [2] E. O. Brimm, J. C. Brantley, J. H. Lorenz, M. H. Jellinek, J. Am. Chem. Soc. 1951, 73, 5427.
- [3] C. G. Granqvist, Handbook of Inorganic Electrochromic Materials, Elsevier Science B.V., Amsterdam 1995.
- [4] S. K. Deb, Appl. Opt. 1969, 8, 192.
- [5] S. K. Deb, Philos. Mag. 1973, 27, 801.
- [6] İ. B. Pehlivan, R. Marsal, E. Pehlivan, E. L. Runnerstrom, D. J. Milliron, C. G. Granqvist, G. A. Niklasson, Sol. Energy Mater. Sol. Cells 2014, 126, 241.
- [7] A. Llordés, G. Garcia, J. Gazquez, D. J. Milliron, *Nature* 2013, 500, 323
- [8] R. Song, G. Li, Y. Zhang, B. Rao, S. Xiong, G. He, Chem. Eng. J. 2021, 422, 130057.
- [9] M. Dontigny, Y. Yang, N. Yu, S. Du, J. Mandal, K. Zaghib, Adv. Funct. Mater. 2018, 28, 1802180.
- [10] C. Xu, G. T. Stiubianu, A. A. Gorodetsky, Science 2018, 359, 1495.
- [11] H.-H. Chou, A. Nguyen, A. Chortos, J. W. F. To, C. Lu, J. Mei, T. Kurosawa, W.-G. Bae, J. B. H. Tok, Z. Bao, *Nat. Commun.* 2015, 6 8011
- [12] W. Bao, J. Wan, X. Han, X. Cai, H. Zhu, D. Kim, D. Ma, Y. Xu, J. N. Munday, H. D. Drew, M. S. Fuhrer, L. Hu, *Nat. Commun.* 2014, 5, 4224.
- [13] K. Takada, R. Sakamoto, S.-T. Yi, S. Katagiri, T. Kambe, H. Nishihara, J. Am. Chem. Soc. 2015, 137, 4681.
- [14] K. Asami, H. Nishi, T. Tatsuma, Nanoscale 2016, 8, 14092.
- [15] P. Joseph, K. Petchimuthu, V. Chinnapiyan, J. Phys. Sci. 2016, 27, 41.
- [16] Q. Hao, Z.-J. Li, C. Lu, B. Sun, Y.-W. Zhong, L.-J. Wan, D. Wang, J. Am. Chem. Soc. 2019, 141, 19831.
- [17] P. Salles, D. Pinto, K. Hantanasirisakul, K. Maleski, C. E. Shuck, Y. Gogotsi, Adv. Funct. Mater. 2019, 29, 1809223.
- [18] J.-f. Feng, T.-F. Liu, R. Cao, Angew. Chem., Int. Ed. 2020, 59, 22392.
- [19] D. Jiang, Bull. Chem. Soc. Jpn. 2021, 94, 1215.
- [20] X. Li, Z. Huang, C. E. Shuck, G. Liang, Y. Gogotsi, C. Zhi, Nat. Rev. Chem. 2022, 6, 389.
- [21] W. Kim, W. Hwang, N. H. Kim, J. Kim, K. Baek, K. Kim, Bull. Chem. Soc. Jpn. 2021, 94, 869.
- [22] J. Song, T. Murata, K.-C. Tsai, X. Jia, F. Sciortino, R. Ma, Y. Yamauchi, J. P. Hill, L. K. Shrestha, K. Ariga, Adv. Mater. Interfaces 2022, 9, 2102241.
- [23] T. Yoshii, K. Chida, H. Nishihara, F. Tani, Chem. Commun. 2022, 58, 3578.
- [24] K. Ariga, S. Watanabe, T. Mori, J. Takeya, NPG Asia Mater. 2018, 10, 90.
- [25] Q. Hao, Z.-J. Li, B. Bai, X. Zhang, Y.-W. Zhong, L.-J. Wan, D. Wang, Angew. Chem., Int. Ed. 2021, 60, 12498.
- [26] F. Yu, W. Liu, S.-W. Ke, M. Kurmoo, J.-L. Zuo, Q. Zhang, Nat. Commun. 2020, 11, 5534.
- [27] D. Bessinger, K. Muggli, M. Beetz, F. Auras, T. Bein, J. Am. Chem. Soc. 2021, 143, 7351.

ADVANCED MATERIALS

www.advancedsciencenews.com www.advmattechnol.de

- [28] R. Sakamoto, K. Takada, T. Pal, H. Maeda, T. Kambe, H. Nishihara, Chem. Commun. 2017, 53, 5781.
- [29] A. Dmitriev, H. Spillmann, N. Lin, J. V. Barth, K. Kern, Angew. Chem., Int. Ed. 2003, 42, 2670.
- [30] S. Stepanow, N. Lin, D. Payer, U. Schlickum, F. Klappenberger, G. Zoppellaro, M. Ruben, H. Brune, J. V. Barth, K. Kern, Angew. Chem., Int. Ed. 2007, 46, 710.
- [31] Z. Shi, N. Lin, J. Am. Chem. Soc. 2009, 131, 5376.
- [32] W. Xu, J.-g. Wang, M. Yu, E. Lægsgaard, I. Stensgaard, T. R. Linderoth, B. Hammer, C. Wang, F. Besenbacher, J. Am. Chem. Soc. 2010, 132, 15927.
- [33] T.-C. Tseng, N. Abdurakhmanova, S. Stepanow, K. Kern, J. Phys. Chem. C 2011, 115, 10211.
- [34] H. Walch, J. Dienstmaier, G. Eder, R. Gutzler, S. Schlögl, T. Sirtl, K. Das, M. Schmittel, M. Lackinger, J. Am. Chem. Soc. 2011, 133, 7909
- [35] T. Kambe, R. Sakamoto, K. Hoshiko, K. Takada, M. Miyachi, J.-H. Ryu, S. Sasaki, J. Kim, K. Nakazato, M. Takata, H. Nishihara, J. Am. Chem. Soc. 2013, 135, 2462.
- [36] T. Kambe, R. Sakamoto, T. Kusamoto, T. Pal, N. Fukui, K. Hoshiko, T. Shimojima, Z. Wang, T. Hirahara, K. Ishizaka, S. Hasegawa, F. Liu, H. Nishihara, J. Am. Chem. Soc. 2014, 136, 14357
- [37] P. Zhang, X. Hou, L. Liu, J. Mi, M. Dong, J. Phys. Chem. C 2015, 119, 28028.
- [38] X. Sun, K.-H. Wu, R. Sakamoto, T. Kusamoto, H. Maeda, X. Ni, W. Jiang, F. Liu, S. Sasaki, H. Masunaga, H. Nishihara, *Chem. Sci.* 2017, 8, 8078.

- [39] K. Wada, K. Sakaushi, S. Sasaki, H. Nishihara, Angew. Chem., Int. Ed. 2018, 57, 8886.
- [40] R. Sakamoto, T. Yagi, K. Hoshiko, S. Kusaka, R. Matsuoka, H. Maeda, Z. Liu, Q. Liu, W.-Y. Wong, H. Nishihara, Angew. Chem., Int. Ed. 2017, 56, 3526.
- [41] M. K. Bera, T. Mori, T. Yoshida, K. Ariga, M. Higuchi, ACS Appl. Mater. Interfaces 2019, 11, 11893.
- [42] Y. Liu, R. Sakamoto, C.-L. Ho, H. Nishihara, W.-Y. Wong, J. Mater. Chem. C 2019, 7, 9159.
- [43] Y. Kuai, W. Li, Y. Dong, W.-Y. Wong, S. Yan, Y. Dai, C. Zhang, Dalton Trans. 2019, 48, 15121.
- [44] S. Mondal, Y. Ninomiya, T. Yoshida, T. Mori, M. K. Bera, K. Ariga, M. Higuchi, ACS Appl. Mater. Interfaces 2020, 12, 31896.
- [45] S. Roy, C. Chakraborty, ACS Appl. Mater. Interfaces 2020, 12, 35181.
- [46] S. Roy, C. Chakraborty, Chem. Commun. 2021, 57, 7565.
- [47] J. Li, X. Wang, W. Sun, K. Maleski, C. E. Shuck, K. Li, P. Urbankowski, K. Hantanasirisakul, X. Wang, P. Kent, H. Wang, Y. Gogotsi, Chem Electro Chem 2021, 8, 151.
- [48] Y. Gogotsi, Q. Huang, ACS Nano 2021, 15, 5775.
- [49] M. Naguib, M. Kurtoglu, V. Presser, J. Lu, J. Niu, M. Heon, L. Hultman, Y. Gogotsi, M. W. Barsoum, Adv. Mater. 2011, 23, 4248.
- [50] B. Anasori, M. R. Lukatskaya, Y. Gogotsi, Nat. Rev. Mater. 2017, 2, 16098.
- [51] G. Valurouthu, K. Maleski, N. Kurra, M. Han, K. Hantanasirisakul, A. Sarycheva, Y. Gogotsi, *Nanoscale* 2020, 12, 14204.
- [52] J. Jiang, L. Qin, J. Halim, P. O. Å. Persson, L. Hou, J. Rosen, Nano Res. 2022, 15, 3587.
- [53] J. Wan, F. Gu, W. Bao, J. Dai, F. Shen, W. Luo, X. Han, D. Urban, L. Hu, Nano Lett. 2015, 15, 3763.



Meng Li obtained his bachelor's degree from Beihang University in 2011 and his master's degree in engineering from China University of Mining and Technology in 2016. Since 2018, he has been a Ph.D. candidate in Prof. Shanqing Zhang's group at Griffith University, Australia. His research interest lies in the study of energy storage materials and stimuli-responsive crystalline smart materials using computational tools.



**Zhenzhen Wu** is a postdoc research fellow at the University of Queensland. Wu obtained her Ph.D. degree in chemistry in late 2021 at Griffith University. She was a postdoctoral research fellow at the Centre for Catalysis and Clean Energy (CCCE) at Griffith University from October 2021 to March 2022. Her research focuses on functional organic materials for electrochemical energy storage. Up to now, she has published over 30 papers in the battery energy field.

and-conditions) on Wiley Online Library for rules of use; OA articles are governed by the applicable Creative Commons License

www.advancedsciencenews.com

www.advmattechnol.de



**Yuhui Tian** received his B.Sc. and M.Sc. degrees from Jiangsu University (China) in 2016 and 2019, respectively. He is currently a Ph.D. candidate under the supervision of Prof. Shanqing Zhang at Griffith University (Australia). His current research interests include the DFT-guided design and synthesis of functional materials for electrocatalysis and rechargeable metal–air batteries.



Feng Pan, chair-professor, VP Peking University Shenzhen Graduate School, founding dean of School of Advanced Materials, director of National Center of Electric Vehicle Power Battery and Materials for International Research, received his B.S. degree from Department of Chemistry, Peking University in 1985 and Ph.D. from Department of P&A Chemistry, University of Strathclyde, UK in 1994. He has been engaged in fundamental research of structure chemistry, exploring "Material Gene" for Li-ion batteries and developing novel energy conversion-storage materials and devices. He also received the 2018 ECS Battery Division Technology Award (US), and 2021 China Electrochemistry Contribution Award.



**Tim Gould** is a theoretical chemical physicist with an interest in method development. His expertise includes a deep understanding of weak van der Waals interactions in 2D and 2D-like materials, which he uses to improve density functional calculations of these difficult-to-model systems. Topics he studies include polymorphism, Moiré heterostructures, and electrochromism. He pioneered the use of random-phase approximation studies of 2D materials, and is co-inventor of the accurate FI/MBD and uMBD van der Waals approximations.



Shanqing Zhang obtained his Ph.D. degree in chemistry in 2001 from Griffith University, Australia. Prof. Zhang has developed and invented a series of patented and commercialized technologies for environmental monitoring and energy storage devices based on functional nanomaterials. He is an Australia Research Council Future Fellow, Fellow of the Royal Society of Chemistry (FRSC), and Fellow of the Royal Australia Chemical Institute (FRACI). Currently, Prof. Zhang is leading a team working on the design and synthesis of nanomaterials and functional polymers for energy conversion and storage devices as well as the development of sustainable and recyclable battery technology.